Nano Energy 77 (2020) 105131

Contents lists available at ScienceDirect

Nano Energy

journal homepage: http://www.elsevier.com/locate/nanoen

Review

Ultrasound-induced wireless energy harvesting: From materials strategies to functional applications

Laiming Jiang [a,b], Yang Yang [c,**], Yong Chen [b,***], Qifa Zhou [a,d,*]

[a] Roski Eye Institute, Keck School of Medicine, University of Southern California, Los Angeles, CA, 90033, USA
[b] Epstein Department of Industrial and Systems Engineering, Department of Aerospace and Mechanical Engineering, Viterbi School of Engineering, University of Southern California, Los Angeles, CA, 90089, USA
[c] Department of Mechanical Engineering, San Diego State University, 5500 Campanile Drive, San Diego, CA, 92182, USA
[d] Department of Biomedical Engineering, Viterbi School of Engineering, University of Southern California, Los Angeles, CA, 90089, USA

ARTICLE INFO

Keywords:
Ultrasound
Wireless energy harvesting
Piezoelectric
Triboelectric
Biomedical
Nanodevices

ABSTRACT

Wireless energy harvesting represents an emerging technology that can be integrated into a variety of systems for biomedical, physical, and chemical functions. The miniaturization and ease of implementation are the main challenges for the development of wireless energy harvesting systems. Unlike most reported wireless energy harvesting technologies represented by electromagnetic coupling, the new generation of ultrasound-induced wireless energy harvesting (UWEH) that use propagating ultrasound waves to carry the available energy provides a strategy with higher resolution, deeper penetration, and more security, especially in nanodevices and implantable medical systems where a long-term stable power is required. Recently, advances in nanotechnologies, microelectronics, and biomedical systems are revolutionizing UWEH. In this article, an overview of recent developments in UWEH technologies that use a variety of material strategies and system designs based on the piezoelectric and capacitive energy harvesting mechanisms is provided. Practical applications are also presented, including wireless power for bio-implantable devices, direct cell/tissue electrical stimulations, wireless recording and communication in nervous systems, ultrasonic modulated drug delivery, self-powered acoustic sensors, and ultrasound-induced piezoelectric catalysis. Finally, perspectives and opportunities are also highlighted.

1. Introduction

With the recent advances in nanotechnologies, microelectronics, and biomedicine, the demand for intelligent electronic systems and wireless power is rapidly increasing [1]. The synergistic effect between nanotechnologies, microelectronics, and biomedicine can be extremely powerful and has played a vital role in a range of applications. For example, implantable biomedical microsystems in the body have recently brought numerous medical advancements in improving the quality of life and extending patient life [2,3]. The implantable biomedical devices (IBDs) are presently applied in various parts of the body as artificial therapeutic means, including cardioverter defibrillators, cardiac pacemakers, artificial retinas, and deep brain stimulators [4,5]. These biomedical electronics can provide real-time diagnosis and treatment towards a variety of diseases associated with the brain, heart, and sensory organs. Advancement in battery technology paved the way for IBDs, but the improvement in storage capacity and service life of batteries is still challenging [6,7]. At present, the battery lifetime is still limited to several years. The surgical interventions for periodically replacing the batteries will prolong hospital stays and place patients at increased risk, such as high morbidity and even mortality [8]. More research and efforts to prolong the service life of the batteries and even eliminate the batteries from the implants, therefore, are required to reduce the medical burden of patients.

New energy harvesting strategies based on self-powered systems have recently been proposed to remove batteries and expand their functionality [9–13]. These systems combine the thermoelectric effect, piezoelectric effect, magnetostrictive effect or electromagnetic induction to integrate energy harvesting devices into the human body for producing electricity from thermal, periodic biomechanical motions (e.

* Corresponding author. Roski Eye Institute, Keck School of Medicine, University of Southern California, Los Angeles, CA, 90033, USA.
** Corresponding author.
*** Corresponding author.
E-mail addresses: yyang10@sdsu.edu (Y. Yang), yongchen@usc.edu (Y. Chen), qifazhou@usc.edu (Q. Zhou).

https://doi.org/10.1016/j.nanoen.2020.105131
Received 25 April 2020; Received in revised form 23 June 2020; Accepted 23 June 2020
Available online 22 July 2020

g., muscle contraction and relaxation, blood circulation, and cardiac motions), or external energy sources outside the body (e.g., inductive energy harvesting and ultrasonic energy harvesting) [14]. Compared with harvesting energy from internal organ motions, wireless external sources can provide tunable and long-term sustainable transmission power, regardless of organ shape, implantation location, and body size. Additionally, wireless energy harvesting enables such implants to operate safely and seamlessly while eliminating the requirement of transcutaneous or percutaneous wire that is cumbrous and prone to infection, especially during long term therapy [15,16].

To date, numerous wireless devices enabling untethered transfer and harvesting have been developed, as well as millimeter-level integrated circuits for bio-implantable systems [17]. Developments over the past few decades have enabled most components in an IBD (including memory, wireless recording and communication systems, oscillators, and electrodes) to be integrated on a tiny chip [18]. In addition, with rapid leaps in technology, a myriad of wireless energy harvesting strategies have been proposed for powering IBDs, such as the mid-field and far-field electromagnetic radiation power, the near-field inductive and capacitive coupling, and ultrasound-induced wireless energy harvesting (UWEH) [15,19]. Each strategy has its own merits and demerits.

The UWEH strategy is to use propagating ultrasound waves to carry the available energy [19]. In contrast to traditional wireless energy harvesting represented by electromagnetic coupling, UWEH has several major advantages. First, the attenuation of ultrasound power in biological tissue is much smaller than the attenuation of electromagnetic radiation. The smaller attenuation will not only realize a longer travel depth at a given power but will also greatly reduce unnecessary energy loss due to tissue absorption or scattering [20,21]. Second, the ultrasonic velocity is several orders of magnitude inferior to radio waves in the tissue, yielding a shorter wavelength at a similar frequency. Smaller wavelengths allow the ultrasonic power to be focused on the size of millimeters point, resulting in an excellent spatial resolution [22,23]. Third, ultrasonic waves are safer in most medical applications [24]. Ultrasound technique has long been used in medical therapeutics and diagnosis [25–27]. According to the regulations of the Food and Drug Administration (FDA), in medical diagnostic applications, the acceptable ultrasound intensity of the human body cannot exceed 720 mW cm^{-2} [28], which is dozens of times greater than the safety threshold of radio waves (1–10 mW cm^{-2}) [29]. Back in 2007, a ZnO nanowire array-based nanogenerator that can be driven by ultrasonic waves to yield continuous electrical output for implantable applications has been proposed by Zhong Lin Wang et al. [30]. Johnson and Seo et al. also developed an ultrasound-induced neural dust micro-system for electrical stimuli and recording of peripheral nerves, which uses ultrasound power and control for downlink communication and readout [20,31]. Consequently, the wireless energy harvesting technology that is ultrasonically induced is a promising strategy in implanted medical systems. In addition, UWEH also provides potential applications in the fields of self-power wireless sensors and chemical catalysis [32–34].

The purpose of this review is to summarize and classify recent developments in UWEH technologies that use a variety of material strategies and system designs for biomedical and chemical functions. First, the energy harvesting mechanism, including ultrasound-induced piezoelectric and capacitive energy harvesting, will be given. Following it, an extensive collection of various types of UWEH systems from the perspective of material strategies (e.g., piezoelectric nanomaterials, piezoelectric films, piezoelectric ceramics and composites, SIO wafers, etc.), fabrication techniques (e.g., MEMS, dice-and-fill method, flexible technologies, etc.), function applications (e.g.,

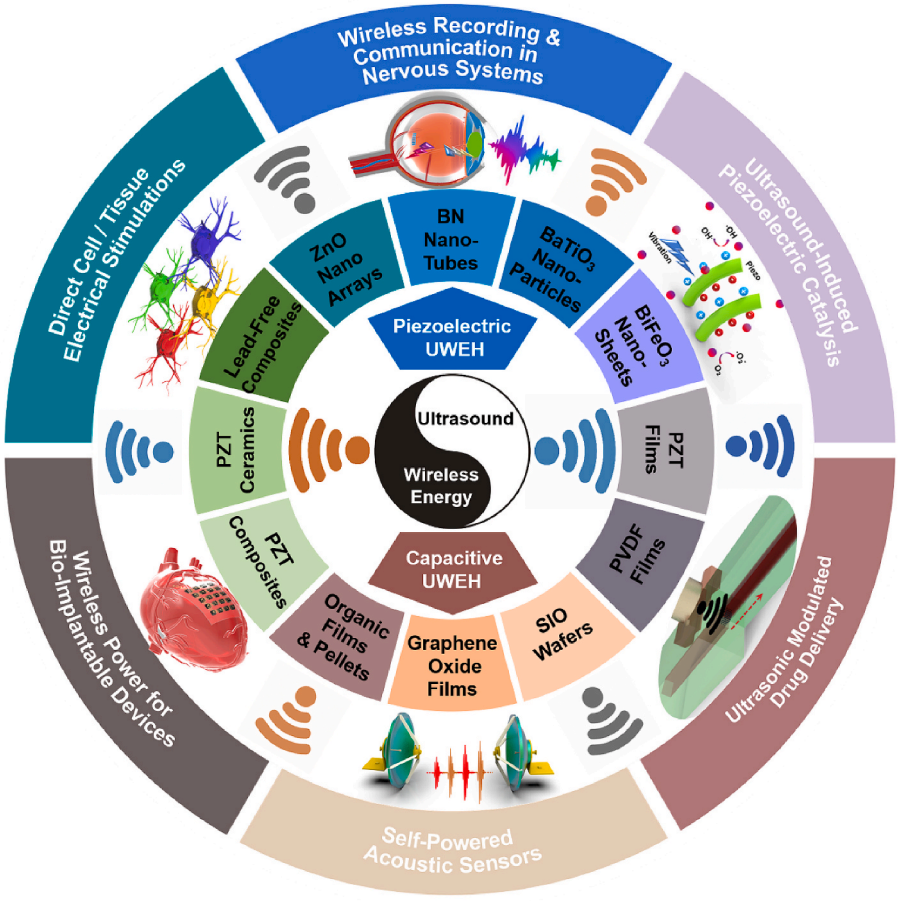

Fig. 1. Integration of ultrasound-induced wireless energy harvesting (UWEH), and the inset shows the categories of materials for UWEH and their applications.

wireless power for bio-implantable devices, direct cell/tissue electrical stimulations, ultrasound-induced piezoelectric catalysis, etc.), and design considerations (e.g., acoustic absorption, acoustic interface and reflection, safety, etc.) will be reviewed and discussed, as summarized in Fig. 1. In addition, opportunities and challenges will also be discussed, and the outlook for future research will be highlighted at the end.

2. Energy harvesting mechanism

Ultrasound is a sound wave with a frequency higher than 20 kHz, which possesses good directivity and is easy to obtain concentrated acoustic energy [35]. The UWEH strategy is to use propagating ultrasound waves to carry the available energy, which is essentially a mechanical vibration that propagates in a host medium [19]. So far, several different energy conversion mechanisms have been proposed for UWEH, which includes: (1) piezoelectric energy harvesting mechanism and (2) capacitive energy harvesting mechanism.

2.1. Piezoelectric energy harvesting

Appling piezoelectric effect to ultrasonic energy has received widespread attention because its diversity of ingenious design can directly convert ultrasonic power into electricity for various integrated applications [19]. The piezoelectric effect originates from the generation of the electric dipole moment in piezoelectric materials (such as ZnO, $BaTiO_3$, lead zirconate titanate (PZT), etc.) that possess a non-centrosymmetric crystal structure and their positive and negative charge centers are under mechanical stress. When a piezoelectric structure is deformed by a mechanical load, such as wind, machine vibration, ultrasonic waves, or human motion, the charge separation process generates a piezoelectric potential that will induce a current to drive electronics (Fig. 2a) [36]. Taking wurtzite-type ZnO nanowires as an example (Fig. 2b and c), the tetrahedrally coordinated atoms (O^{2-} and Zn^{2+}) are stacked layer by layer along the *c*-axis [37,38]. In their initial state, the charge centers of the cations and anions overlap each other. If an external force is applied, the configuration will be distorted (stretched or compressed). Consequently, the positive and negative charge centers will be separated and procedure an electric dipole resulting in piezopotential. When an external circuit is connected to the distorted piezoelectric body, the induced charges will be driven to screen the piezopotential and flow through the external electrodes to achieve a new equilibrium. Thus, the electrical signal flowing through the external circuit is consecutively produced as the piezopotential is sequentially altered via exerting a dynamic pressure. This main mechanism of piezopotential is applicable to a variety of piezoelectric materials. The piezoelectric UWEH system mainly consists of piezoelectric elements and an ultrasound source. The two core issues in developing piezoelectric UWEH are material selection and system structural design.

2.2. Capacitive energy harvesting

2.2.1. Electret-based electrostatic energy harvesting

The electrostatic energy harvesting device is based on variable capacitor structures that can be biased either via pre-charged electret materials or an external voltage source [39,40]. The electrostatic energy harvesting devices have received tremendous attention due to its compatibility with the integrated circuit (IC) and microelectromechanical systems (MEMS) [41]. These devices can be summarized into two types. One is an electret-free electrostatic energy harvester that uses a conversion cycle consisting of charging and discharging of a capacitor. However, active electronic circuits are needed to impose the charging cycles on the structure and must be synchronized with the change in capacitance. The other is the electret-based electrostatic energy harvester that applies electrets, enabling them to directly convert mechanical energy into electricity. An electret is a dielectric with long-lasting charges [42]. For example, silicon oxide is a common

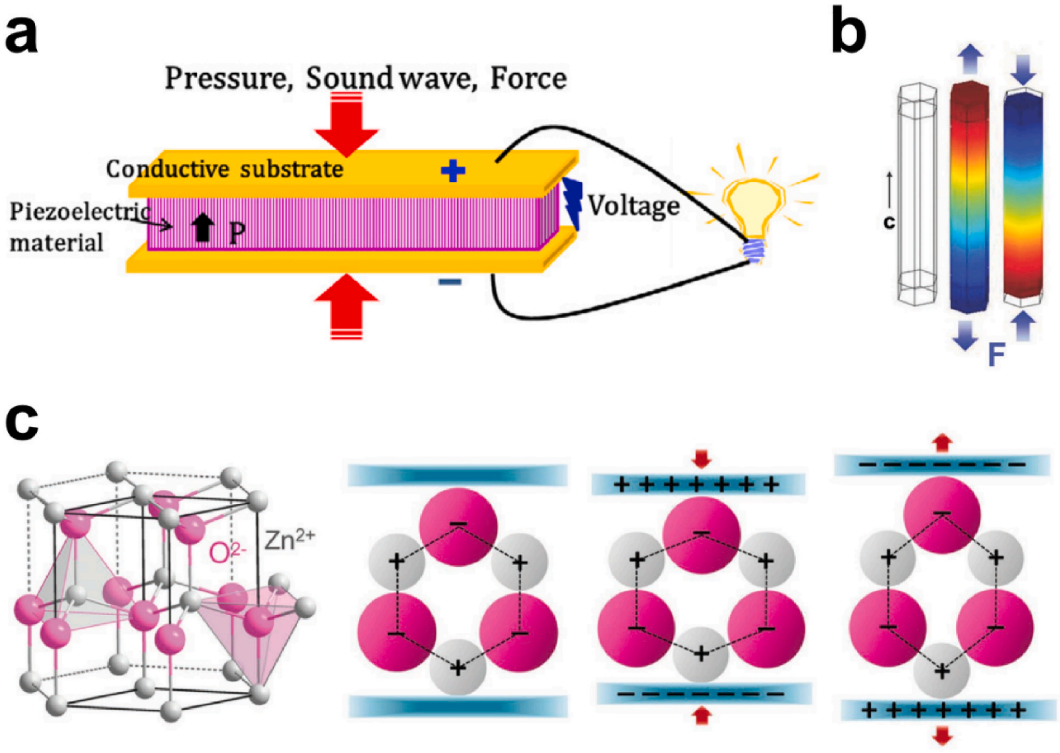

Fig. 2. Mechanism of piezoelectric energy harvesting. a) Schematic of a piezoelectric energy harvesting device. Reproduced with permission [36]. Copyright 2018, Elsevier. b) Simulation of the piezoelectric potential distribution in a ZnO nanowire under axial strain. Reproduced with permission [37]. Copyright 2009, AIP Publishing LLC. c) Atomic model and the different piezopotential in tension and compression modes of the wurtzite-structured ZnO. Reproduced with permission [38]. Copyright 2017, Wiley-VCH.

inorganic electret material [43]. As shown in Fig. 3a, the electret-based harvesting device is based on a variable capacitive architecture consisting of two conductive sheets (counter electrode and electrode). The electret will induce charges on the electrode and counter electrode, which follows Gauss's law. The relative displacement of the counter electrode compared to the electrode and the electret will induce a change in the geometry of the capacitor and results in the reorganization of charges between the counter electrode and the electrode through the external load *R* (Fig. 3b) [44]. The process leads to a current circulation through the external load and hence the mechanical energy is converted into electrical energy.

2.2.2. Triboelectric energy harvesting

The well-known triboelectric effect is essentially an electrically charging phenomenon when different materials are in frictional contact [38]. Although this is one of the most common phenomena in our daily life, until recently, the essential fundamental understanding of the process was relatively limited. It is generally believed that chemical bonds are formed between certain parts of the surfaces of the different contacted materials, and charges will shift from one surface to another because of the different ability to obtain electrons. The charges shifted between two surfaces could be electrons, ions, and molecules. As the two surfaces are separated, some bonded atoms tend to retain the shifted charges, while others tend to release them, which may induce the opposite electrostatic charges on two different friction surfaces. The induced opposite charges on both friction materials will produce a triboelectric potential that can drive a flow of electrons in the external circuit to equilibrium the resulting potential drop. When an external load is connected, a current is formed that flows from one electrode to another. Then, the potential difference between the two surfaces will change when the two surfaces are in contact again, causing the current flowing backward (Fig. 3c and d) [45]. Since the first triboelectric nanogenerator (TENG) was reported by Zhong Lin Wang in 2012 [46], the development of the capacitive triboelectric technology has made it promising not only in common electronic components but also in implantable biomedical UWEH applications [47].

3. Piezoelectric UWEH: Materials and designs

3.1. Piezoelectric nanomaterials-based UWEH

Piezoelectric nanomaterials are ideal for many energy harvesting related applications due to their inherent small size and unique mechanical and electrical properties [48]. The small size of nanomaterials makes them suitable for applications where space is limited, such as implantable medical nanodevices. Fewer materials are needed to manufacture nanostructures, and the synthesis method can be highly scalable [49]. Nanomaterials may also possess favorable electrical properties not inherent in the bulk materials, such as enhanced piezoelectric factor and elastic modulus [50,51]. Numerous nanogenerators with different architectures have been developed and progressive improvements in performance have led to their integration into various nanodevice systems.

3.1.1. Zinc oxide (ZnO) nano-arrays

Since the first report of the ultrasound-induced ZnO-based nanogenerator by Zhong Lin Wang's group in 2006 [30], UWEH has become a novel wireless energy transmission strategy, especially in implantable bioelectronics [52,53], because it can offer a mobile, adaptable, and cost-effective strategy for harvesting energy from external sources. In addition, one-dimensional zinc oxide (ZnO) nanostructures (e.g., nanobelts and nanowires) have become one of the most important piezoelectric materials because ZnO is an environment-friendly, stable, and versatile material that holds a broad vision of applications in fields of sensors, nanoelectronics, photocatalysis, and energy harvesting [51, 54–56].

Specific to Wang's work aforementioned (Fig. 4a) [30], the proposed ultrasonic nanogenerator is composed of vertically aligned ZnO nanowire arrays (NWs) that can generate continuous current output through ultrasonic waves. The NWs were grown on a GaN substrate coated with a

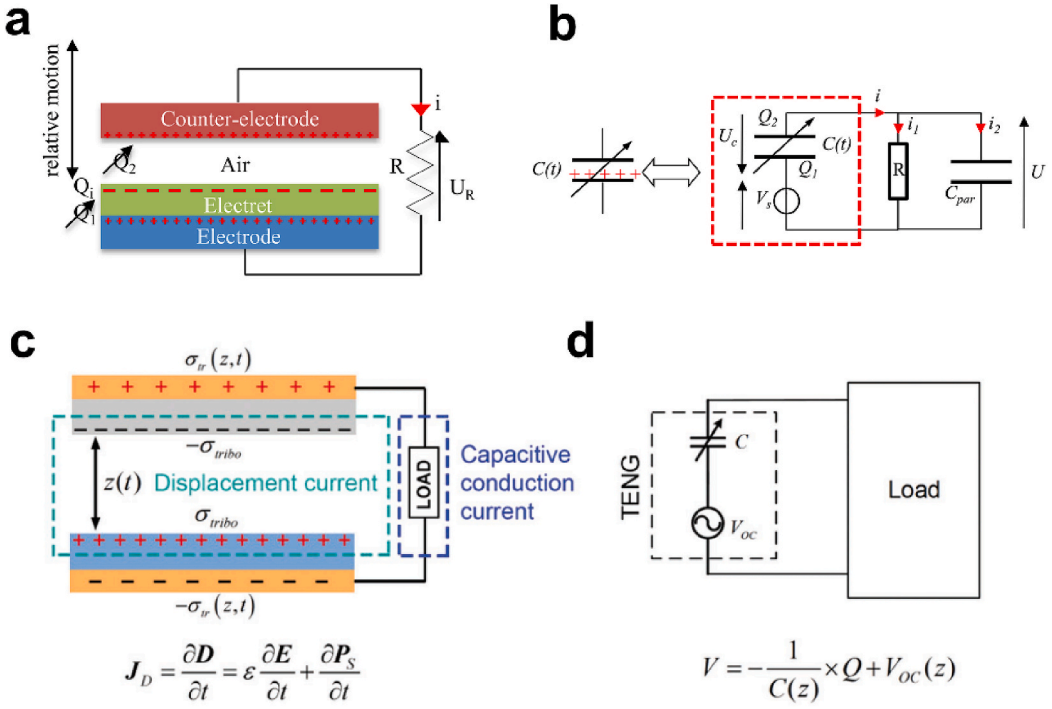

Fig. 3. Mechanism of capacitive energy harvesting. a) Schematic of the electret-based electrostatic energy harvesting. b) The equivalent circuit of the electret-based electrostatic energy harvester. Reproduced with permission [44]. Copyright 2012, IntechOpen. c) Schematic of the working mechanism of the Triboelectric energy harvesting. d) The equivalent circuit of the TENG. Reproduced with permission [45]. Copyright 2018, Wiley-VCH.

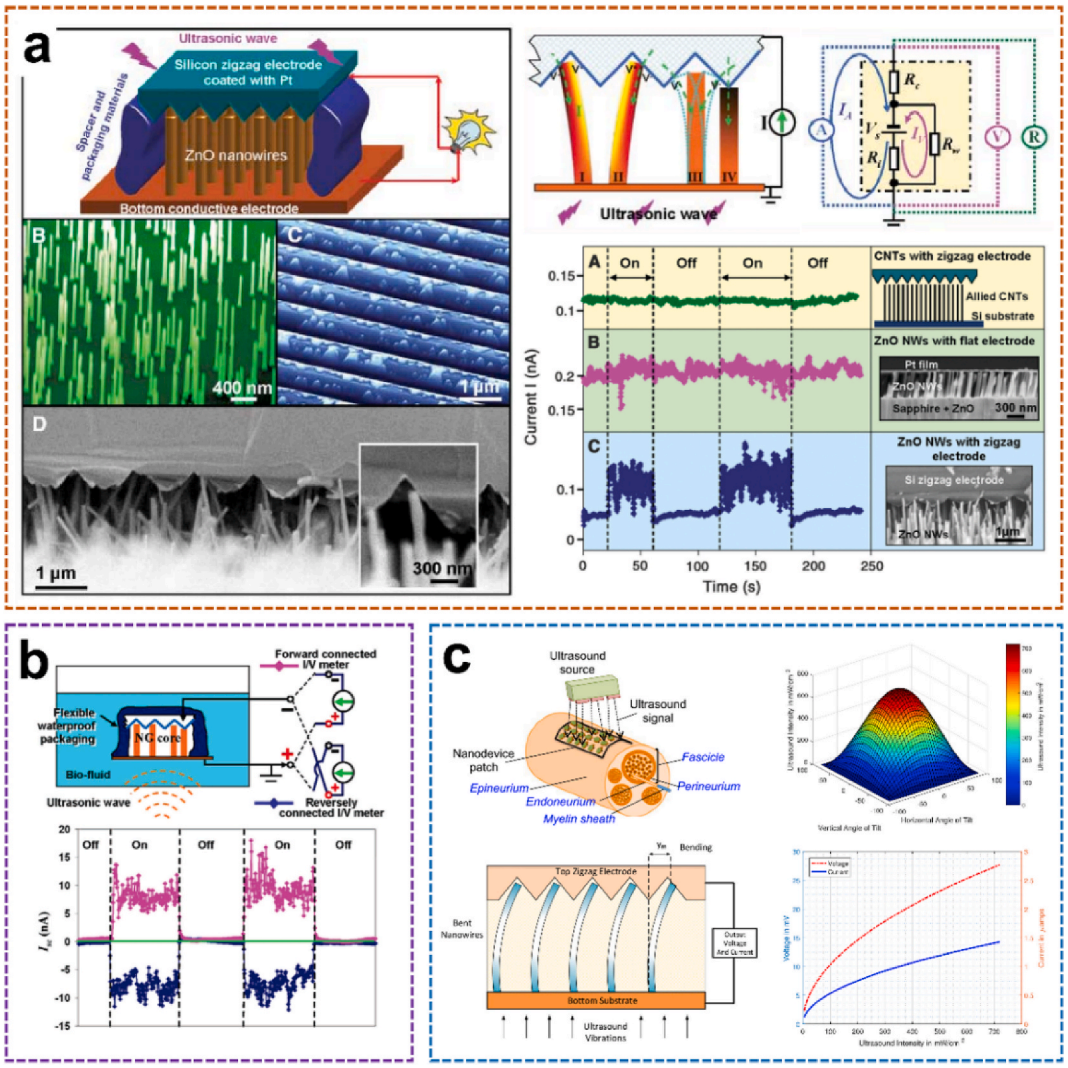

Fig. 4. ZnO nano-arrays-based UWEH. a) A ZnO nanowire-based nanogenerator driven by ultrasonic waves. Reproduced with permission [30]. Copyright 2007, American Association for the Advancement of Science. b) Integrated nanogenerator that operates in biofluid. Reproduced with permission [57]. Copyright 2007, American Chemical Society. c) Nanodevice arrays for peripheral nerve fascicle activation. Reproduced with permission [59]. Copyright 2017, Institute of Electrical and Electronics Engineers.

thin layer of ZnO film, which served as a common electrode that directly connects the arrays to an external circuit. The NWs were then covered by parallel zigzag Si trenches that were coated with a thin layer of platinum as the top electrode. The diameter and length of each nanowire are 1 μm and 40 nm, respectively, and the density of the NWs are 10 μm^{-2}. In order to ensure appropriate contact between the NWs and the electrode, the resistance of the nanogenerator has been monitored by turning the spacing between the electrode and the NWs. The encapsulated equipment is fixed on a metal sheet that is in direct contact with the water in the cavity of the ultrasound transmitter. Once the ultrasonic-driven NWs touch adjacent tooth, the Schottky barrier between the electrode/nanowire interface will be forward-biased and piezoelectric discharge will occur, thereby observing the current in the external circuit. The current and voltage output signals of the nanogenerator were measured with the transmission ultrasonic wave of 41 kHz being turned on and off periodically. A current jump of 0.15 nA was detected as the ultrasound was turned on, and the signal instantly dropped to the baseline once the ultrasound was turned off. The voltage output showed a similar trend with a maximum negative signal of approximately −0.7 mV. The generated power of each nanowire driven by ultrasound was 1–4 fW. The output density per NW is about 1–4 W cm^{-3}. Additionally, the measured resistance of the entire nanogenerator remains extremely stable ($R = 3.560 \pm 0.005$ kΩ) with and without turning on the ultrasound. The output current of the nanogenerator is reasonably stable and continuous for an extended period of more than 1 h. It provides a potential strategy to power nanodevices and integrated nanosystems.

Additionally, the developed ZnO-nanowire based nanogenerator was further optimized, and its performance was characterized inside biofluid under ultrasonic stimulation (Fig. 4b) [57]. During the characterization process, the current and voltage meters were successively forward and reversely connected to the two electrodes of the 2 mm^2 size nanodevice. The corresponding short-circuit current (I_{sc}) and open-circuit voltage (V_{oc}) signals were observed, respectively. After the ultrasound was switched on, the current output peaks up to 17 nA with an average value of 9 nA and a "noise/instability" within ±4 nA. The corresponding voltage output is about 0.1 mV. In addition, the output current was improved by 20–30 times and achieved as large as 35 nA as the nanodevice was placed at an ultrasound focused area. A systematic study of the output of a similar ultrasonic-driven ZnO nanogenerator in a confined tube was also conducted [58]. These two studies unambiguously show the feasibility of UWEH for power conversion inside biological fluids or any other type of liquid.

With the advance of the nano ZnO-based UWEH technologies, an implanted nanodevice array for selective stimuli of peripheral nerves in

the human body was further proposed [59]. as shown in Fig. 4c. ZnO-based nanoarrays are embedded into a polymer-based patch of biocompatible tissue and placed close to the outer layer of the nerve. The device harvests the energy from ultrasonic waves emitted by a portable external transmitter. The harvested ultrasonic energy is then converted by the ZnO nanoarrays and emits electronic impulses that stimulate nerve bundles through the electrodes. The maximum ultrasonic energy will be delivered to the nanoarrays if the acoustic beam is perpendicular to the device and thus hits the entire array area. Generally, the incident acoustic intensity will be decreased if the nanoarrays are tilted at an angle to the ultrasonic beam. And the relationship between the output signal of the nanoarrays and the ultrasound intensity is approximately linear. Therefore, based on the selection of patch arrays consisted of nanowires, the main competitive advantage of the proposed strategy is the capability of selectively stimulating nerve bundles at different locations and depths (e.g., peripheral nerve pundles) to avoid interfering other sensory fascicles by adjusting the intensity of the incident ultrasonic waves or spatially targeting specific nanoarrays on the synthetic patch. It demonstrates a longer-term implantation solution for selective neural stimulation *in vivo*, which ensures patients greater freedom of movement compared to embedded tethered electrodes.

3.1.2. Boron nitride nanotubes (BNNTs)

Boron nitride nanotubes (BNNTs) are the structural analogs of carbon nanotubes (CNTs) with superior mechanical, chemical, and electrical properties [60]. The alternating N and B atoms completely replace the C atoms in the graphite-like flakes without changing the atomic spacing. In recent years, BNNTs have been proved to have excellent piezoelectric properties [61,62]. The theoretical calculation and experimental research of piezoelectric properties and spontaneous polarization of BNNTs show that BNNTs is a piezoelectric system with excellent performance, and its response value is larger than that of piezoelectric polymer, which is equivalent to that of wurtzite semiconductor. Therefore, similar to the above-mentioned ZnO-based nanogenerators that produce a continuous current through ultrasonic waves, BNNTs could also be exploited as nano transducers that provide output currents for direct electrical stimulation applications [63].

An ultrasound-assisted piezoelectric wireless stimulation of neuronal-like cells was successfully performed for the first time by Gianni Ciofani et al. using BNNTs (Fig. 5a) [64]. The BNNTs with a typical "bamboo-like" structure and with a dimension of about 50 nm in diameter and about 200–600 nm in length were first dispersed and stabilized by glycol chitosan, yielding a stable glycol chitosan-BNNT dispersion. After that, PC12 cells were cultured in glycol chitosan-BNNTs (0–100 μg mL^{-1}) containing medium for up to nine days. The results showed that BNNTs did not induce obvious oxidative stress production in PC12 cells even after 9 days of incubation at high BNNTs concentrations. Additionally, differentiating status (the proportion of differentiated cells in culture), neurite length, and the number of neuronal processes per cell were also monitored in cultures incubated with different amounts of BNNTs, both nonstimulated and stimulated with ultrasonic waves. It is worth noting that the number of neuronal processes per differentiated cell increased obviously in BNNTs-incubated and ultrasound-stimulated cultures. Compared to the general four processes in the control groups, about five processes were observed on average in BNNTs-ultrasound stimulated cultures. No significant differences were observed between the various BNNTs concentrations studied. However, the most obvious result is a significant increment in neurites due to the combined stimulation. The average neurite length in the BNNTs-ultrasound combined cultures was distinctly longer than that of the control groups after 72 h of treatment, and this increment increased by approximately 30% at the end of the day 9. As a result, an external wireless ultrasound source can be employed to deliver electrical stimuli to tissue or cell cultures internalized by piezoelectric BNNTs.

Besides the ultrasound-induced piezoelectric direct electrical stimulation, the combination of chemical, mechanical, topographical, and intracellular electrical stimulation based on UWEH on a co-culture of skeletal muscle cells and fibroblasts was also studied by Ricotti et al. (Fig. 5b) [65]. First, functional free-standing polyacrylamide gels with different topography as petri dishes for cell culture were prepared. Then, they co-cultured murine myoblasts and normal dermal human fibroblasts on these dishes with supplementing BNNTs and outside ultrasound sources. BNNTs were internalized by murine myoblasts and localized in both early and late endosomes without being internalized by the underneath fibroblast layer. The co-culture characteristics were enhanced through intracellular electrical stimulation induced by piezoelectric BNNTs activated by ultrasounds. The differentiation of myoblasts benefited from the synergistic effects of chemical, mechanical, topographical, and ultrasound-induced BNNTs-mediated stimulation, showing good myotube development (longer, thicker and more functional) and alignment towards a preferential orientation, along with a high expression of genes encoding key proteins for muscle contraction (i.e., myosin and actin). A greater functionality of the intracellular electrical stimulated co-cultures was experimentally demonstrated. The response to the aforementioned ultrasound-induced piezoelectric physical stimulation in terms of cytokine production and gene expression was also clarified. More results and discussions can be found in the literature [65].

3.1.3. Barium titanate nanoparticles (BTNPs)

Several *in vivo* and *in vitro* researches have proved that electrical

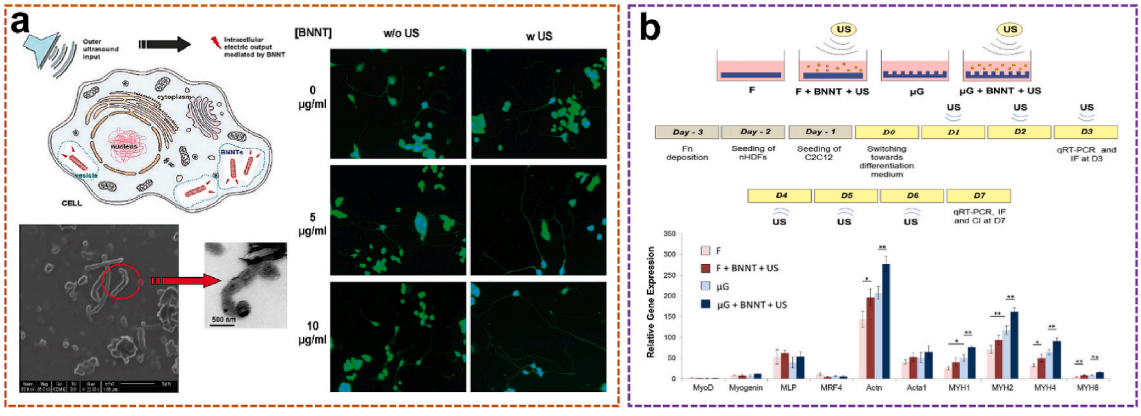

Fig. 5. BNNTs-based UWEH. a) Enhancement of neurite outgrowth in neuronal-like cells following BNNTs-mediated stimulation. Reproduced with permission [64]. Copyright 2010, American Chemical Society. b) Cell co-culture on micro-engineered hydrogels based on BNNTs-mediated stimulation. Reproduced with permission [65]. Copyright 2013, Public Library of Science.

stimulus plays a significant role in the regeneration of transected nerve ends and neurite extension [66–68]. Electrical charges appear to be concentrated in stimulating axonal regeneration. Piezoelectric nanomaterials and UWEH technology offer innovative methods for neuron stimulation. Thus, more and more piezoelectric nanomaterials have been evaluated to determine whether they can be applied to effective nerve regeneration [69]. For example, an intensive study has been performed on the neural stimulation of SH-SY5Y-derived neurons based on the effects of ultrasound-induced barium titanate nanoparticles (BTNPs) by using imaging methods for detecting the Ca^{2+}/Na^{+} fluxes (Fig. 6a) [70].

The piezoelectric medium chosen here was the typical tetragonal BTNP with perovskite-like crystallographic structure. First, BTNPs functionalized with gum Arabic possess quite a well-dispersed structure. The hydrodynamic dimension of the BTNPs characterized by dynamic light scattering was 479.0 ± 145.3 nm, and the polydispersity index was 0.180. BTNPs are visible through confocal fluorescence imaging that was performed to evaluate the interaction between BTNPs and neurons. In particular, BTNPs (in red) were detected associated not only with the membrane (in green) of the cell bodies but also with their neurites (Fig. 6a). The researcher monitored the intracellular Ca^{2+} dynamics in response to the ultrasound stimulation conducted at various acoustic intensities with or without BNTPs. The results demonstrated that the combination of BTNPs and an ultrasonic intensity of 0.8 W cm^{-2} can induce high-amplitude Ca^{2+} transients ($\Delta F/F0$ peak = 0.62 ± 0.12) in H-SY5Y-derived neurons, clearly higher than all other control groups, including the case with ultrasound at 0.8 W cm^{-2} but without BTNPs. Additionally, Ca^{2+} imaging research was carried on with the addition of blockers of the voltage-gated Na^{+} channels (tetrodotoxin, TTX) and the voltage-gated Ca^{2+} channels (Cd^{2+}) to explore the observed Ca^{2+} transient ion channels. Interestingly, these high-amplitude Ca^{2+} transients were successfully suppressed by both the TTX and the Cd^{2+} actions, indicating that the generation of the high-amplitude Ca^{2+} transients by the ultrasound combined with BTNPs stimulation was mediated by both Na^{+} and Ca^{2+} voltage-gated channels. The phenomenon was further observed in the experiment of Na^{+} imaging experiments under the same conditions. It is worth mentioning that Ca^{2+} waves are known to play a significant role in promoting the maturation of the neural networks, particularly by regulating the growth of neurites. In this regard, as Gianni Ciofani et al. have previously shown how the UWEH-based piezoelectric stimulation can effectively promote the neurite elongation [64].

In addition to promoting higher functionality of the stimulated cell cultures, the UWEH-based piezoelectric stimulation to inhibit the proliferation of cancer cells has also been explored. Marino et al. have investigated this approach to inhibit the proliferation of breast cancer cells (Fig. 6b) [71]. The innovative solution includes a biocompatible and functionalized piezoelectric BTNPs-based platform that targets and remotely stimulates HER2-positive breast cancer cells. UWEH-driven anti-proliferative effects of BTNPs-assisted stimulation greatly decreased proliferation by regulating cell cycle arrest. Similar to low-intensity AC electric fields, UWEH-based chronic piezoelectric stimulation was able to inhibit cancer cells proliferation by up-regulating the expression of the genes encoding Kir3.2 inward rectifying potassium channels, by interfering with the homeostasis of calcium ions, as well as by influencing the organization of mitotic spindles during mitosis. The reported approach shows great potential and versatility in treating different types of cancer. Future research will focus on functionalizing piezoelectric nanoparticles with specific molecules to target piezoelectric particles to membranes of specific cell types.

3.1.4. *$BiFeO_3$ nanosheets*

Studies have shown that bismuth ferrite ($BiFeO_3$) is a promising catalyst for hydrogen production through photocatalytic water decomposition because of its good chemical stability and narrow band-gap (~ 2.2eV) [72–74]. In addition, $BiFeO_3$ is also ferroelectric and piezoelectric material with a huge spontaneous polarization of more than 100 μC cm^{-2} and a large piezoelectric constant (d_{33}) of about 100 p.m.·V^{-1} [75,76]. Analogous to photocatalysis, where the photo-induced electric charges (electron-hole pairs) participate in the catalytic redox reactions, in theory, piezoelectric charges (positive and negative ones) induced by periodic mechanical vibration can also be applied to activate catalytic redox reactions, which can be called piezocatalysis [77,78]. Therefore, based on the piezoelectric charges induced by mechanical vibrations, UWEH was introduced for piezo-catalytic hydrogen production and dye decomposition via hydrothermally synthesized $BiFeO_3$ square nanosheets (Fig. 7) [34]. $BiFeO_3$ nanosheets were prepared here to realize high catalytic activity because the small dimension and large surface area of nanosheets facilitate rapid charge transfer between the redox couples and the catalyst. The as-synthesized $BiFeO_3$ catalyst possessed a morphology of square nanosheet with a normal direction of $[001]_{pc}$ and an average dimension of ~380 nm (Fig. 7a).

$BiFeO_3$ nanosheets with a typical rhombohedral phase are

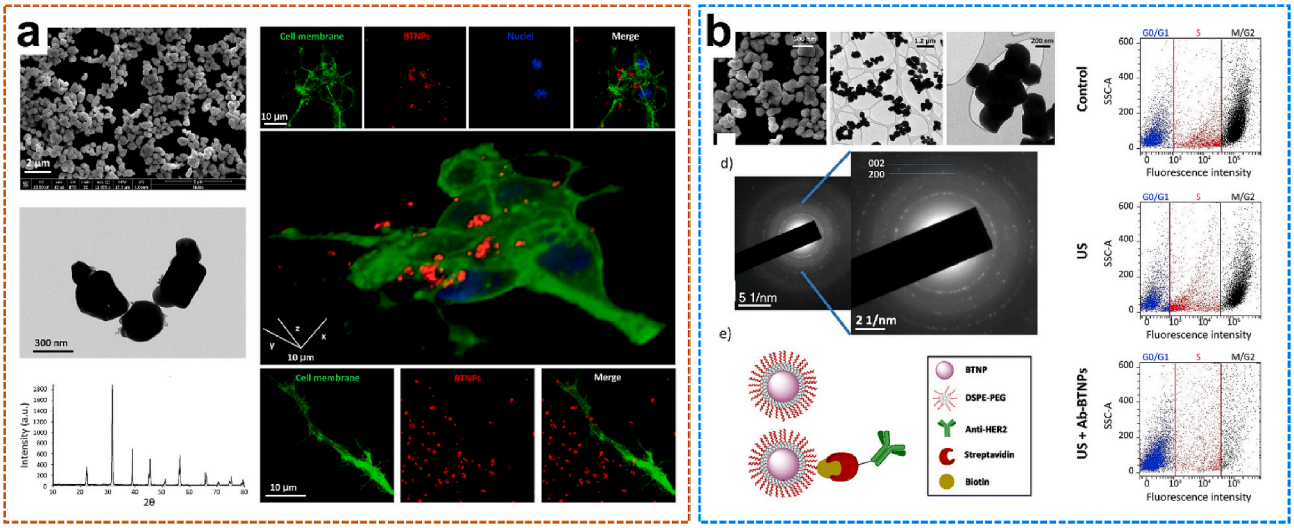

Fig. 6. BTNPs-based UWEH. a) Piezoelectric BTNPs-assisted wireless neuronal stimulation. Reproduced with permission [70]. Copyright 2015, American Chemical Society. b) Ultrasound-activated piezoelectric BTNPs inhibit the proliferation of breast cancer cells. Reproduced with permission [71]. Copyright 2018, Nature Publishing Group.

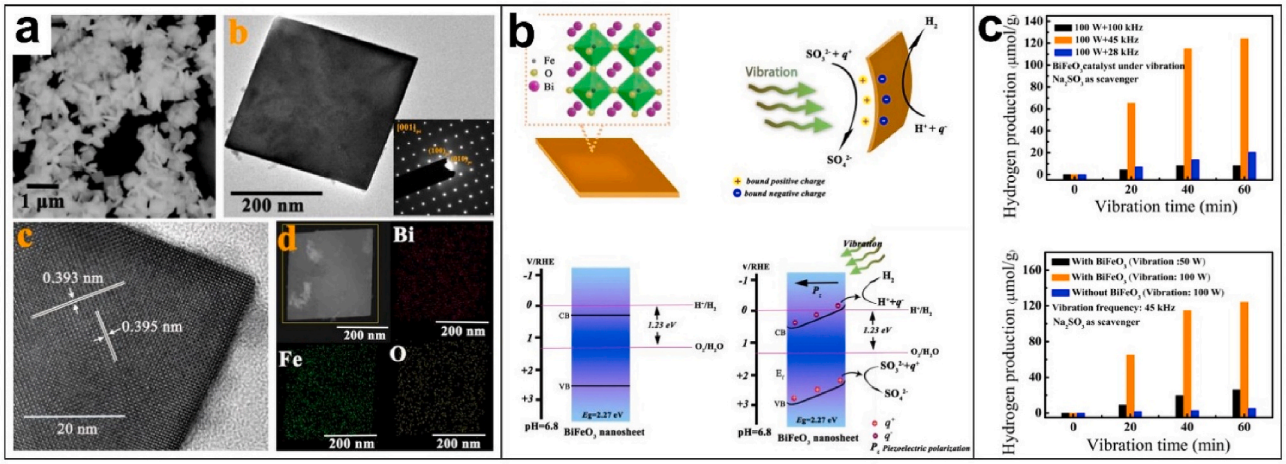

Fig. 7. $BiFeO_3$ Nanosheets-based UWEH. a) Morphology characterizations of the $BiFeO_3$ nanosheets. b) Schematic illustration of the ultrasound-induced piezoelectric catalysis mechanism and tilting of energy bands. c) The piezoelectric catalytic hydrogen production. Reproduced with permission [34]. Copyright 2019, Wiley-VCH.

ferroelectric and piezoelectric because of the non-central symmetry of their *3 m* point group. Here, these thin $BiFeO_3$ nanosheets will bend when subjected to mechanical stress. Accordingly, numerous positive and negative charges will be produced on the surface of the nanosheet due to the piezoelectric effect. The negative charges (q^-) produced on the surface of the $BiFeO_3$ nanosheet will effectively combine with the dissociated hydrogen ions (H^+) in the water to generate H_2. In the meantime, the sacrificial agents (SO_3^{2-}) will consume the positive charges (q^+) generated on the other side of the nanosheet. It should be noted here that the flat band potential of the prepared nanosheet is 0.32 V and the bandgap is approximately 2.27 eV. The results also show that the piezoelectrically induced internal electric field was able to slope the conduction band and enable the catalytic hydrogen evolution reaction. According to calculations, the slope of the conduction band leads to the band edge to be raised on the negatively charged side, which is slightly negative than the H_2/H_2O redox potential (0 V) for hydrogen evolution reaction (Fig. 7b). Thus, the piezo-catalytic hydrogen production in water can be achieved on pure $BiFeO_3$ nanosheets. Additionally, the capability of piezocatalysis can be effectively tuned via the variation of nanosheet geometry and material properties.

The piezo-catalytic hydrogen generation results demonstrated that the total hydrogen generation per gram of nanosheets is as high as 20.4, 124.1, and 8.3 μmol, respectively, when the ultrasonic frequencies are 28, 45, and 100 kHz, and the ultrasonic power is 100 W for 1 h (Fig. 7c). The resonance frequency of the synthesized $BiFeO_3$ nanosheet is calculated to be approximately 46.5 kHz. This result indicates that the optimal piezo-catalytic hydrogen production was attained near the resonance frequency of the piezoelectric nanosheet, where the mechanical vibrational energy was more efficiently transferred to electricity. Additionally, higher ultrasonic power results in higher hydrogen generation. The relationship between the piezoelectric factor (d), the acoustic stress (T), and the piezoelectric charges (Q) per unit area on the nanosheet can be summarized as $Q = d \cdot T$. Higher ultrasonic power leads to higher stress T and produces more charges on the surfaces of the catalyst, yielding a higher hydrogen generation rate. The piezo-catalytic effect of the nanosheets was also performed for dye decomposition. The piezo-catalytic decomposition ratio of Rhodamine B dye reached 94.1% after ultrasonically powering for 50 min and the Rhodamine B dye solution became almost completely transparent. This is an important development to demonstrate that the potential of UWEH for piezo-catalytic hydrogen production via nano piezoelectric materials, innovatively expanding the feasibility of using UWEH in more general applications.

3.2. Piezoelectric films/diaphragms-based UWEH

With the development of high integration and complexity of electronic systems, it is necessary to integrate more components on smaller substrates [79,80]. Therefore, the development of miniaturized and films/diaphragms-based devices is a feasible way to reduce the overall volume and weight of the system. Additionally, the films with flexibility provide the benefit of strong mechanical compliance, and thus can be used as flexible devices [81]. For this reason, the films/diaphragms will contribute to the realization of thin, pliable, and lightweight UWEH devices that enable the harvesting of transmitted ultrasound under the skin and at interfaces of organs for electricity.

3.2.1. PZT films/diaphragms

PZT, or $PbZr_xTi_{(1-x)}O_3$, is one of the most common piezoelectric material, which is favored by researchers because of its superior electromechanical coupling coefficient over many other piezoelectric systems such as PVDF and $BiFeO_3$ [5,82]. In 2014, He et al. reported a small-sized, implantable UWEH device based on PZT film that was realized using a MEMS-based technology (Fig. 8a) [83]. The MEMS-based process could eliminate the size limitation (1–100 μm) of the piezoelectric films, thereby increasing the electrical output of the energy devices. Additionally, MEMS is capable of integrating multiple sensors with different sensitive directions and different functions to form a micro-sensor array [84,85]. In He's work, a 40 μm-thick PZT film was first prepared through bonding and mechanically thinning process. The natural frequency of the UWEH device was then adjusted by optimizing the side length and thickness of the silicon film and cavity [86]. The whole UWEH device is wire bonded on a printed circuit board (PCB) substrate. The final manufactured size of the device is $5 \times 6 \times 0.5$ mm^3 with a resonant cavity of 3.24×3.24 mm^2. Subsequently, the output properties were measured in water and *in vitro* tissue. Under the ultrasonic excitation frequency of 40.43 kHz, the UWEH device demonstrates an optimal output power of 35 μW at an acoustic power density of 3.7×10^{-9} J cm^{-3}, a load resistor of 1.3 kΩ, and a receiving distance of 20 mm in water. Meanwhile, an optimal power of 49 μW was achieved at the acoustic power density of 1.25×10^{-8} J cm^{-3} and a receiving depth of 22 mm in a piece of fresh pork tissue. Correspondingly, the pressure sensitivity of the UWEH device is approximately 0.296 mV Pa^{-1}, indicating favorable output properties.

Recently, also based on the MEMS process, Shi et al. presented a broadband UWEH device, which was enabled by a PZT diaphragm array and used as a self-powered implantable medical device (Fig. 8b) [87]. The device composed of 7 PZT diaphragms that are of a miniaturized dimension with an optimized width-to-length ratio and are connected in

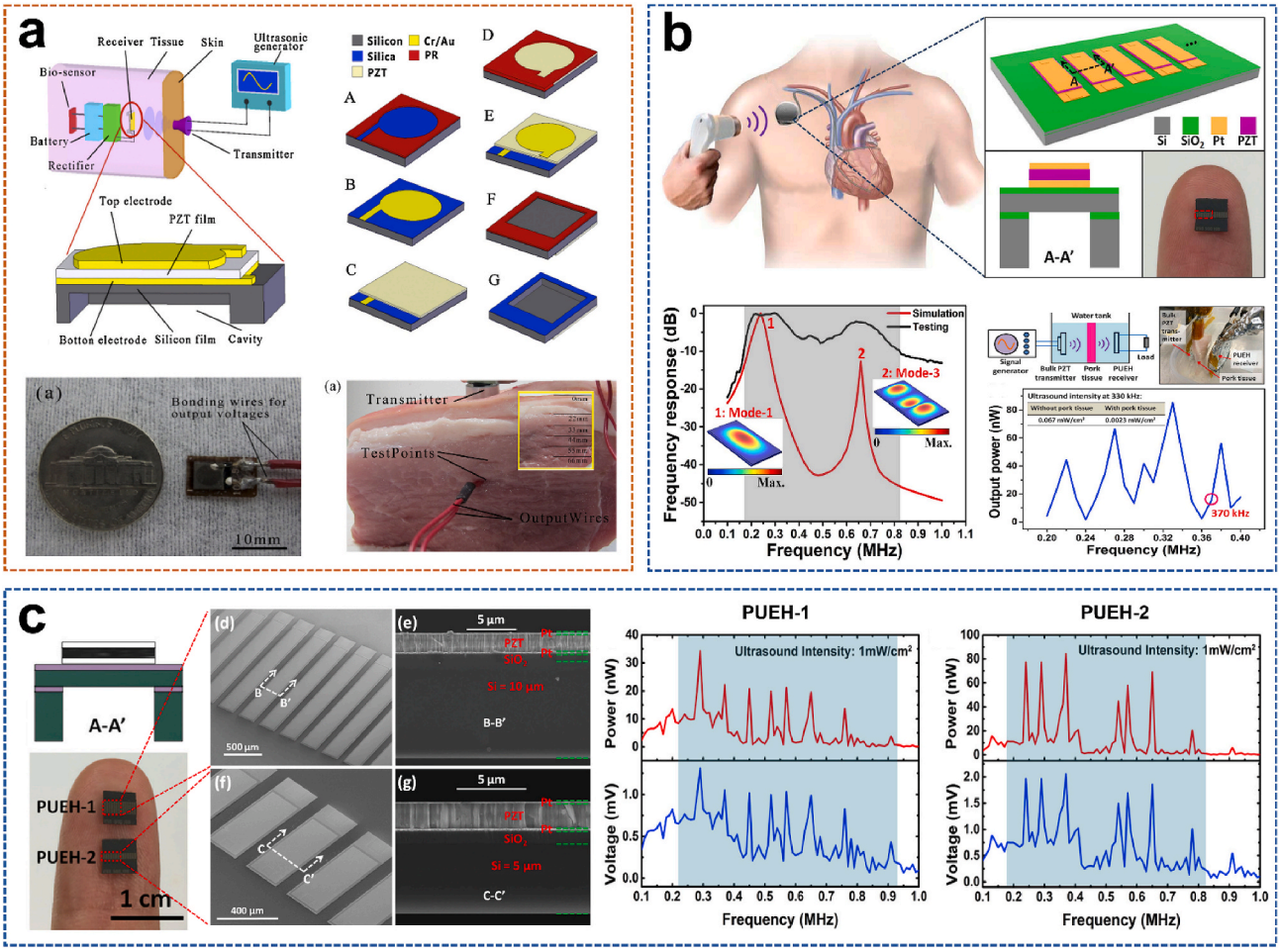

Fig. 8. PZT films/diaphragms-based UWEH. a) A PZT film-based UWEH device fabricated by the MEMS process. Reproduced with permission [83]. Copyright 2014, Elsevier. b) PZT diaphragm array-based harvester for enabling self-powered implantable biomedical devices. Reproduced with permission [87]. Copyright 2016, Nature Publishing Group. c) Investigation of geometric design in PZT diaphragms for UWEH. Reproduced with permission [88]. Copyright 2016, AIP Publishing LLC.

parallel to improve the output power. The size of each PZT diaphragm is 250 μm × 500 μm with a multilayered structure, where the PZT layer is 2 μm. The space between the two diaphragm elements is 90 μm. The effective size of the whole device is 2.058 mm^2. The results show that a broad bandwidth of the UWEH device is from 170 kHz to 820 kHz. In addition, distance fluctuation caused by standing wave effect can be avoided in a wide range by altering different ultrasonic frequencies for the fluctuated distance. For example, the *in vitro* testing of the UWEH device to harvesting ultrasonic energy through pork tissue demonstrated that the output power was only 16.5 nW when the ultrasonic frequency is 370 kHz, and then the output power was improved to 85.2 nW by adjusting the ultrasonic frequency to 330 kHz. The distance between the ultrasonic transmitter and the harvester was 23 mm, and the thickness of the pork tissue was 6 mm.

In order to improve the output characteristics, the same research group also presented a study on geometric design in MEMS-based piezoelectric diaphragms for ultrasound energy harvesting (Fig. 8c) [88]. These presented PZT diaphragm-based piezoelectric ultrasound energy harvesters (PUEHs) possess the same structure, but with different dimensions. The PZT diaphragms in PUEH-1 and PUEH-2 are 250 μm × 1550 × 2 μm and 250 μm × 500 μm × 2 μm, respectively. The effective total areas for PUEH-1 and PUEH-2 are 4.67 mm^2 and 2.06 mm^2, respectively. Both PUEHs possess excellent broadband performance due to the aspect ratio and thickness design. PUEH-1 possesses a wide - 6 dB bandwidth of 74.5% with a center frequency of 350 kHz. However, PUEH-2 possesses two wide - 6 dB bandwidth of 73.7% and 30.8% with center frequencies of 285 kHz and 650 kHz. The maximum output power at ultrasonic intensity input of 1 mW cm^{-2} was 34.3 nW and 84.3 nW for PUEH-1 and PUEH-2, respectively. The corresponding power density was 0.734 μW cm^{-2} and 4.1 μW cm^{-2}, respectively. As a result, PUEH-2 exhibits much better power output characteristics and relatively wider operating bandwidth due to the optimized aspect ratio and thickness design, which gives a feasible design scheme for improving the energy harvesting efficiency of implantable UWEH devices.

A comparative investigation of the design configurations of two bio-implantable UWEH architectures (bulk-mode PZT plate and flexure-mode PZT diaphragm) has also been conducted [89]. Generally, the total power produced from each of the UWEH architectures is a function of their aspect ratio, diameter, and implanted depth. The results demonstrated that the plate and diaphragm architectures as implants in muscle can produce equivalent amounts of power for device dimensions in the millimeter level. However, for device dimensions in the sub-millimeter level, the flexure-mode diaphragm architecture typically produces higher power than the bulk-mode plate one and is noticeably less sensitive to variations in implanted depth.

3.2.2. *PVDF films*

Currently, most polymer-based piezoelectric generators are fabricated from polyvinylidene fluoride (PVDF) and its copolymers of trifluoroethylene (PVDF-TrFE), nylon-11, and polyuria [90]. These kinds of polymer materials intrinsically have a piezoelectric effect. The merits of PVDF are its ease of processing, lead-free composition,

vibration-sensitive, lightweight, smoothness, low density, and low acoustic impedance (~4 MRayl) that facilitates acoustic impedance matching with media such as water (~1.5 MRayl) and biological tissue (~1.7 MRayl) [91,92]. Additionally, it is flexible, with high elastic compliance, and thus can be easily attached to the surface of concave-convex structures [93,94].

A thin-film-based UWEH device for medical micro-robot designed to operate in the blood vessels, such as in an artery, has been reported (Fig. 9a), with a particular focus on the manufacturing of co-axial PVDF nanofiber thin-films as converting components to enhance conversion efficiency and facilitate electrodes preparation [95]. Aligned co-axial nanofibers with a diameter of 500 nm in the UWEH device are prepared by a direct drawing method with co-axial micro-pipettes between designed locations. PVDF is made into the nanofiber shells with a core consisting of conductive polyaniline (PANI). Both ends of the nanofiber array are cut into anodes by Au mass. An Al film covering the nanofiber array by a sputtering process is the cathode. The entire cantilever is coated with a biocompatible polymer film (polyurethane) to facilitate the ability to operate *in vivo*. The nanofilm-based energy harvesting cantilever components were then fixed on a cylindrical micro-robot to form a medical device that can be manipulated ultrasonically in a blood vessel. In order to analyze whether the nanofiber cantilever structure can generate sufficient power to maintain the normal operation of the micro-robot, the resonance frequency of the nanofiber cantilever and the optimal output power under the different length of the cantilever (l) and Au mass (l_a) were estimated. The maximum amount of cantilever for a cylindrical structure is 20 when considering a 3 μm wide cantilever and a 20 μm diameter micro-robot in an artery. Assuming that the ultrasonic intensity I_0 is 1 W cm^{-2} that is safe for the human body [96], the cantilever is perpendicular to the ultrasound propagation direction, and the ultrasound is completely reflected, the results clearly showed that the micro-robot can yield much more power than 1 μW as the parameters were properly selected [97]. When l_a is 1 μm and l is 25 μm, the calculated output power can achieve to 100 μW, which is very promising to provide sufficient power for the micro-robot in the artery to maintain its movement. Higher power may be produced if more cantilever layers are integrated into the micro-robot along with the cylindrical body.

Another novel UWEH scheme for a bio-implantable autonomous active stent (AAS) based on the patterned PVDF-film has also been reported (Fig. 9b) [98]. The device was specifically designed for percutaneous coronary intervention (PCI). The stent can harvest energy from ultrasonic waves and power a series of implantable sensors and microelectronic devices, which was expected to revolutionize the current PCI mode by not only eliminating the bare wire stents but also monitoring and preventing the failures. The UWEH device composed of 50 μm-thick PVDF films with a corrugated surface pattern that was designed to tolerate expansion. This pattern also helps the stent to promote the enhancement of surface vibration. Compared to the ordinary PVDF film, the autonomous active stent with tightly placed surface patterns showed a higher output power (14.8% improvement). The stent with a diameter of 10 mm and a length of 30 mm can generate 230 μW of electrical energy with an efficiency of 11.5% when exposed to 14 MHz ultrasound. The results demonstrated that the patterned autonomous active stent has excellent potential for use as medical implants placed in different locations inside the human body.

3.3. Piezoelectric ceramics and composites-based UWEH

Ceramic materials account for approximately 87% of the total piezoelectric market because of their simple preparation process and desirable comprehensive acoustic and electrical properties [99], especially the lead-based perovskites represented by PZT ceramics. For example, the commercial PZT-5H has a piezoelectric coefficient d_{33} that can easily reach 650 pC/N [100]. Lately, Li et al. reported a rare-earth-doped $Pb(Mg_{1/3}Nb_{2/3})O_3$–$PbTiO_3$ ceramic with Giant d_{33} value of up to 1500 pC/N [101], making the performance of lead-based ceramics unmatched by other piezoelectric systems. Nevertheless, significant progresses have also been made in the development of lead-free materials as well as their devices due to environmental considerations [27,99,102–105].

3.3.1. PZT ceramics

Owing to the relative convenience of obtaining ceramics with high performance and various geometric shape, untethered ultrasonic neural dust motes base on small (~170–250 μm^3) PZT piezoceramic cubes for cortical recording were proposed by Seo et al. [106], as shown in Fig. 10a. This extremely compliant and ultra-miniature system, which consists of low-power electronics coupled with ultrasound power transmission and backscatter communication, enabled significant scaling in the number of neural recordings from the brain while providing access to a truly chronic brain-computer interface. The assembly sensor nodes were realized on a two-layer printed circuit board (PCB) where metalized PZT cubes of various dimensions (~170–250 μm^3) were attached to the pre-soldered bump electrodes using solder paste. Neural dust motes immersed in water 30 mm away from the ultrasonic interrogator couple with 0.04246 ppm backscatter and

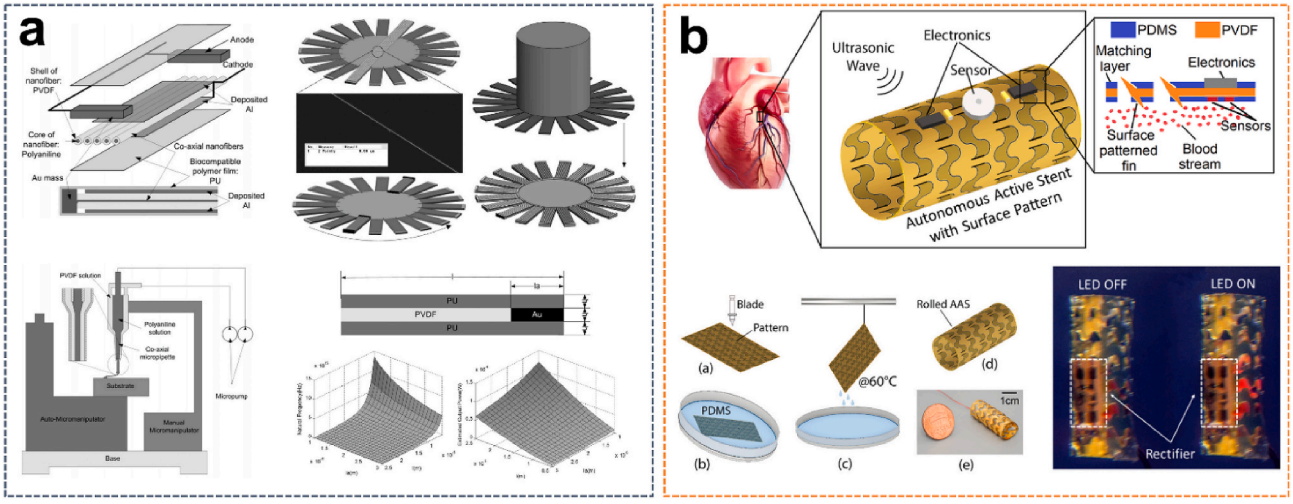

Fig. 9. PVDF films-based UWEH. a) PVDF nanofiber film-based UWEH device for an artery micro-robot. Reproduced with permission [95]. Copyright 2011, Elsevier. b) Patterned PVDF film-based UWEH scheme for an implantable active stent. Reproduced with permission [98]. Copyright 2018, Institute of Electrical and Electronics Engineers.

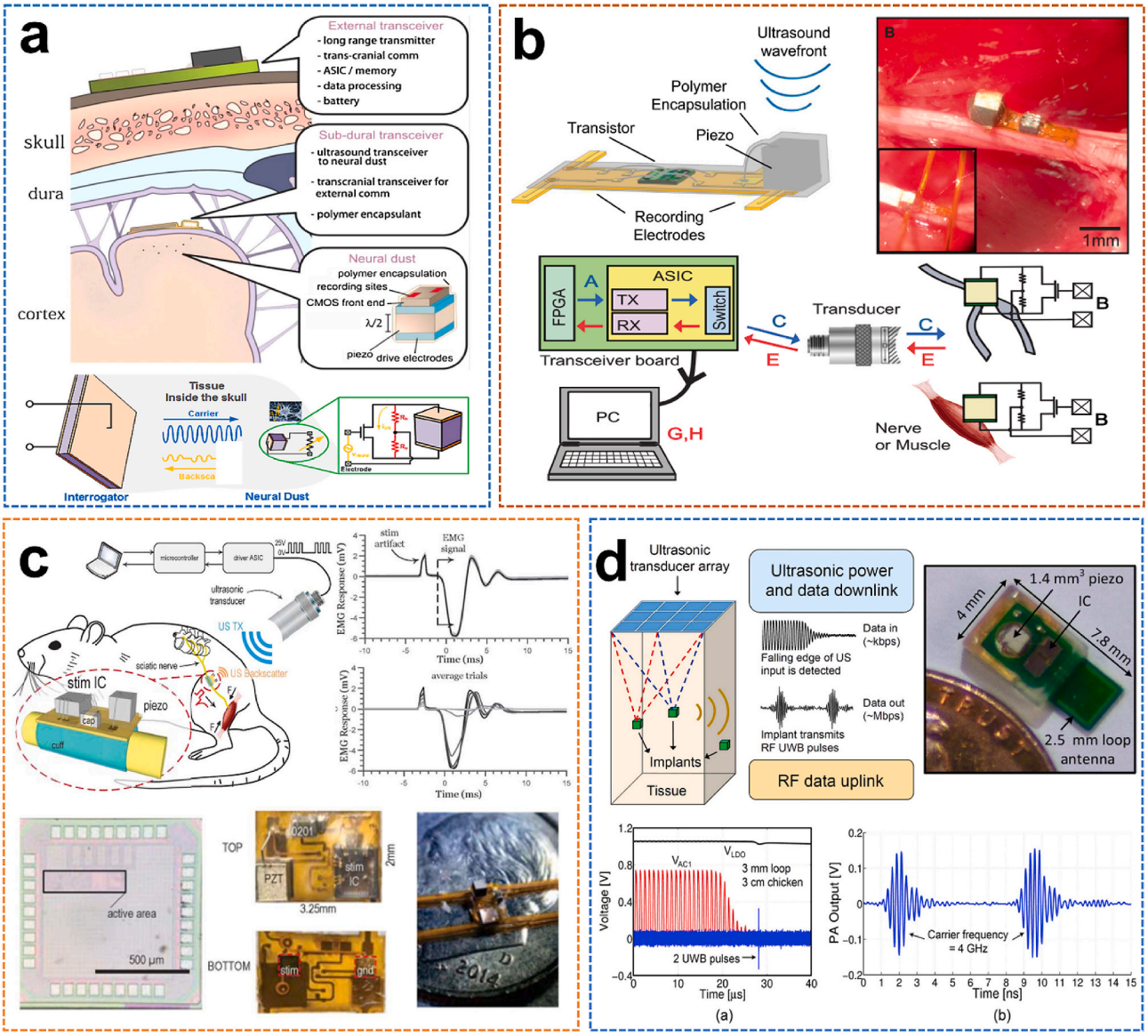

Fig. 10. PZT ceramics-based UWEH. a) PZT ceramic-based micro UWEH device for neural dust motes of cortical recording. Reproduced with permission [106]. Copyright 2015, Elsevier. b) Wireless recording in the peripheral nervous system using a PZT ceramic-based UWEH device. Reproduced with permission [20]. Copyright 2016, Elsevier. c) A PZT-based UWEH device for wireless peripheral nerve stimulator. Reproduced with permission [31]. Copyright 2018, Institute of Electrical and Electronics Engineers. d) A mm-sized implantable device with wireless power transfer and a hybrid bi-directional data link based on a PZT ceramic-based UWEH device. Reproduced with permission [107]. Copyright 2015, Institute of Electrical and Electronics Engineers.

0.002064% power transfer efficiency, yielding a maximum received power of about 0.5 µW with 1 nW of change in backscatter power with neural activity. Additionally, the experimental results indicate that the high efficiency of wireless ultrasonic transfer can enable the scaling of the sensor nodes down to, at least, about100 µm scales and possibly even lower.

Similar to the aforementioned strategy, the same research group further developed PZT piezoceramic-based ultrasonic neural dust motes for wireless recording in the peripheral nervous system (Fig. 10b) [20]. The emerging field of bioelectronic medicine is seeking new solutions to decrypt and regulate electrophysiological activity in the human body to achieve therapeutic effects in target organs. Current technologies that interface with muscles and peripheral nerves rely heavily on wires. Moreover, traditional electrode-based approaches lack the capability of recording from the nerve with a high spatial resolution or recording independently from many discrete locations within the nerve bundle. This work presented the new neural dust, a scalable and wireless ultrasound backscattering system, can power and communicate with mm-scale bio-implanted bioelectronics. The neural dust implant was integrated on a 50-mm-thick flexible polyimide PCB, where both the custom transistor (0.5 mm × 0.45 mm) and the PZT piezo material (0.75 mm × 0.75 mm × 0.75 mm) were bonded to the top side of the PCB. The measurement results showed that the neural dust mote on the axis could convert incident ultrasonic power into electricity across the load resistance with an efficiency of about 25%. Battery-free and passive communication using backscatter enabled the high-fidelity transfer of electroneurogram (ENG) and electromyogram (EMG) signals in anesthetized rats. Both the peak-to-peak voltages of the EMG and ENG display a S-type response as a function of stimulus power. The minimum signal recorded by a neural dust mote is about 0.25 mV.

Recently, Johnson et al. also presented a PZT-based wireless peripheral nerve stimulator with a whole dimension of 6.5 mm^3 and a mass of 10 mg (Fig. 10c) [31]. The encapsulated stimulator is controlled and powered through ultrasonic waves from an external transmitter and

utilized a single piezoelectric block for downlink communication, powering, and readout. Peak efficiency of 82% at an average stimulation current of 48 μA was achieved when it converted harvested ultrasound to stimulation charge. The measured DC power was 4 μW when not stimulating. The small and light stimulator was also tethered to the sciatic nerve of an anesthetized rodent at a depth of 21.5 mm and exhibited a full nerve activation *in vivo*. In addition, another millimeter-level implantable piezoelectric stimulator with ultrasound power transmission and a hybrid bi-directional data communication link (Fig. 10d) was also presented by Charthad et al. [107]. A hybrid data link composing of ultrasound downlink and radiofrequency uplink was presented in this design. The implantable device was 4 mm × 7.8 mm in size and consisted of a PZT ceramic-based UWEH device, an IC, and an off-chip antenna, supporting a maximum measurable DC load power of 100 μW. As a result, these mm-sized UWEH devices based on small piezoceramic blocks reveal several outstanding advantages and tremendous potential for remarkable electrical stimulators and communicator candidates for *in vivo* medical devices.

3.3.2. PZT 1–3 composites

The performance of composite materials may be superior by combining the desirable structures of two different phases, such as a 1–3 composite with a structure of piezoelectric pillars aligned in the passive polymer matrix [108–110]. This composite possesses a lower acoustic impedance (Z_a), a higher coupling coefficient (k_{33}), a lower loss, and better design flexibility [111,112]. Moreover, 1–3 piezoelectric composites can excite almost pure thickness-tensile vibration near the resonance frequency, which indicates that this structure is one of the best candidate designs for harvesting longitudinal ultrasound energy [113]. Theoretical analysis and experimental measurement of a 1–3 piezoelectric composite-based ultrasonic harvester operating with thickness-tensile modes have been implemented [114]. The 1–3 composite harvester was manufactured by aligning PZT ceramic pillars in a passive resin matrix. Both surfaces of the composite device were electroded, and the electrodes are connected to an external circuit whose impedance is denoted by Z_L. When Z_L increases infinitely ($\rightarrow +\infty$), which implies an open circuit, and when the load resistance is equal to the impedance of the harvester, the maximum output power dissipated in the load can be realized. The harvested power was also studied experimentally through the use of the 1–3 PZT/epoxy composite disc. The highest power was 0.189 W when the driving frequency was near the fundamental resonance and the load Z_L (100 Ω) was almost equal to the impedance of its resonance frequency. The corresponding energy density was calculated to be 300 mW cm^{-3}. This model provides a valuable guideline for exploring the optimization of the device design, operating frequency, and matched load impedance.

Additionally, Sun and co-workers proposed a wideband UWEH device using a 1–3 piezoelectric composite with a non-uniform thickness (Fig. 11a) [115]. This harvester was designed and processed to be a PZT/epoxy flat-concave disk, and the thickness of the piezoelectric rods along the radial direction gradually increases, so that the arrays possess overlapping frequency spectra with the maximum powers at similar but different frequencies. The difference in frequency Δf (resonance frequency and resonance frequency) was broadened significantly because of the parallel-connected rods of varying thicknesses, which is different from the conventional piezoelectric devices having a uniform thickness. Correspondingly, the operating frequency range (~0.6 MHz - 1.2MHz) of the presented device was broadened significantly. The maximum open-circuit voltage within the passband harvested was about 3.6 V. The output power dissipated in the optimal load (Z_L = 160 Ω) was approximately 2.5 mW.

In addition to the choice of materials, the structural design of the device is also a noteworthy consideration, especially in bio-implantable applications. The surfaces of tissues or organs in the human body, such

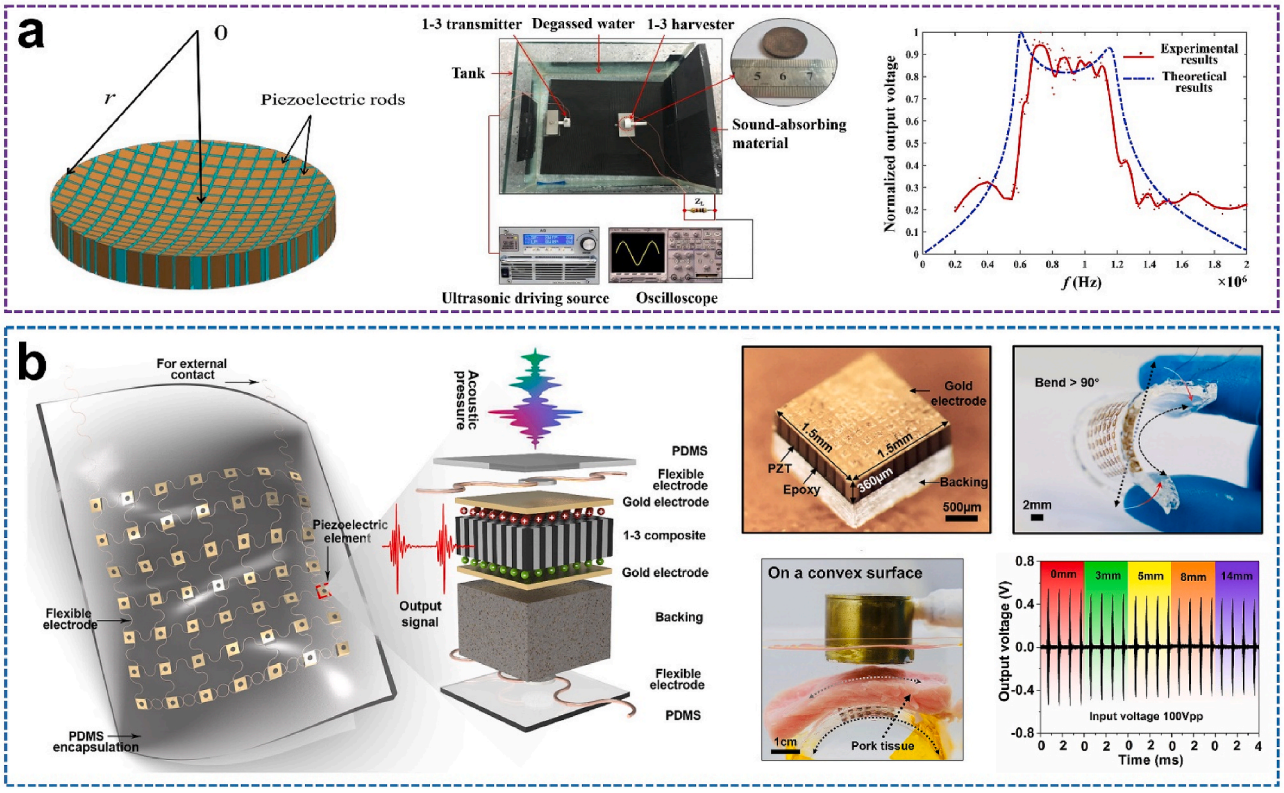

Fig. 11. PZT 1–3 composites-based UWEH. a) A wideband energy harvester using 1–3 piezoelectric composite with nonuniform thickness. Reproduced with permission [115]. Copyright 2018, AIP Publishing LLC. b) PZT piezoelectric composite-based flexible UWEH array. Reproduced with permission [116]. Copyright 2018, Elsevier.

as the heart, intestine, blood vessels, brain, and eyeball are always complex and concave-convex. Traditional energy harvesting devices are mostly rigid. Therefore, they are limited for such tissues or organs because of incongruent contact with curved or corrugated surfaces. The latest progress in the development of flexible energy devices is an important impetus for solving the aforementioned issues [5,103,116,117]. Fig. 11b shows our recent work of a flexible piezoelectric ultrasound energy harvesting array made by integrating numerous piezoelectric components with multilayer flexible electrodes [116]. The device employs a 7 × 7 piezoelectric array of small size and high performance 1–3 PZT/epoxy composites as core elements (1.5 mm × 1.5 mm footmark with a space of 1.5 mm), multilayered corrugate copper wires as electrical interconnects, and an elastomer film (PDMS) as the encapsulation. The overall thickness of the as-manufactured harvester is about 2 mm. The harvester shows good flexibility that can be seamlessly attached to the curved surfaces and realize a curvature of more than 90°. With these unique features, the flexible UWEH array can be excited by ultrasound to generate continuous electrical outputs on both curved and planar surfaces. The output current and voltage signals produced from the UWEH array reached more than 4 μA and 2 Vpp, respectively, with a power of 4.1 μW cm^{-2}. The rectified energy can be stored in capacitors and then is sufficient for lighting commercial LED without additional power. In the *in vitro* test for bio-implantable application, output signals exhibit very weak attenuation properties (≤15%) even when the thickness of the mimicked implanted tissue increased from 0 to 14 mm, showing a promising application scheme in the bio-implantable system for flexible UWEH technologies.

3.3.3. *Lead-free 1–3 composites*

As mentioned above, lead-based piezoelectric ceramics represented by PZT ceramics and their related lead-based solid solutions dominant the most piezoelectric market due to their excellent electrical properties [99,118]. However, there has been a concern in recent years that these lead-based piezoelectrics containing toxic ingredients are harmful to human body, especially in the medical field where the direct and intimate contact with the human body is usually required [27,119,120]. Meanwhile, there is an increased social awareness of environmental protection and a directive released on Restriction of the Hazardous Substances (RoHS) [121], making it imperative to develop new eco-friendly lead-free materials and devices as lead-based alternatives.

Recently, our collaborators and we proposed a novel retinal electrical stimulation scheme using the lead-free-based UWEH technique to wirelessly power millimeter-scale implants (Fig. 12) [103]. The as-developed bio-implantable device hybridizes high-performance microscale lead-free piezo-composite with a flexible structural frame. The schematic and optical images of the device are shown in Fig. 12a and b, respectively. As the core element of the device, a (K,Na)NbO_3 ceramic-based lead-free 1–3 type piezo-composite with the microstructure of 85 μm piezo-pillars and 25 μm kerfs was designed and manufactured by a modified dice-and-fill process to achieve improved electrical and acoustic properties (Fig. 12c). At present, (K,Na)NbO_3 has been developed into the most promising candidate for the lead-based ones due to its outstanding ferroelectric/piezoelectric properties and bio-friendly properties [122–127], which are essential for biomedical applications. As a result, the fabricated piezo-composite exhibited a reduced acoustic impedance (Z_a ≈ 11.6 MRayl) and a resonant frequency of 6.06 MHz. The longitudinal electromechanical coupling k_{33} (≈0.70) and voltage coefficient g_{33} (≈38.3 × 10^{-3} V m N^{-1}) were significantly enhanced by suppressing shear vibration mode and reducing the dielectric constant in the composite structure [128,129], effectively improving the sensitivity of the piezo-composite to sense ultrasonic waves. The integrated piezo-element with a backing layer (~300 μm) possesses a spatial dimension of 1 mm × 1 mm × 0.6 mm, connected by flexible electrodes and encapsulated in an elastomer silicone.

Systematic investigations, including numerical simulation, frequency characteristics, load optimization, input conditions, and implanted mimic, were conducted to evaluate output characteristics of the device and to validate its feasibility in practical applications. The flexible device can conform to complex surfaces and be excited by ultrasound to generate a tunable electrical output, achieving a maximum instantaneous power density of 45 mW cm^{-2} at a load resistance of 1 kΩ.

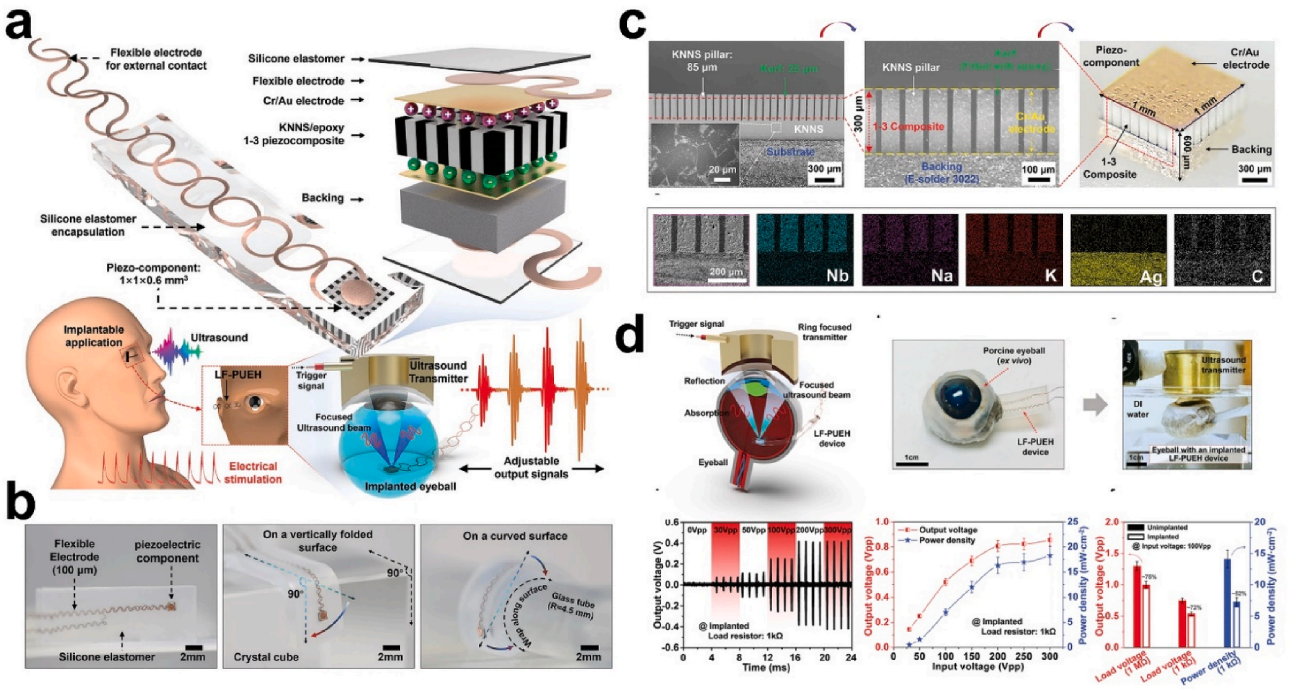

Fig. 12. Lead-free composites-based UWEH. a) Schematic of the lead-free UWEH device. b) Optical images of the lead-free UWEH device when standing freely and wrapped a vertically folded surface and a curved surface. c) Fabrication and microstructure of the lead-free composite component. d) *Ex vivo* test of the lead-free UWEH device. Reproduced with permission [103]. Copyright 2019, Wiley-VCH.

An *ex vivo* test implanted in the porcine eyeball was performed to demonstrate the feasibility of implanting the device in the body (Fig. 12d). There was a slight drop in the output amplitude of the device in the implanted environment. For example, the output voltage reached 0.54 Vpp at the input amplitude of 100 Vpp and a load of 1 kΩ, and the corresponding power density was 7.3 mW cm^{-2}, which are 72% and 52% of the values in the non-implanted case, respectively. Additionally, the significant current signals (e.g., current density > 9.2 nA μm^{-2}, and current > 72 μA), which are larger than the average thresholds required for retinal electrical stimulation, were also detected in the *ex vivo* test. This work laid the foundation for the next generation of the implantable electrical stimulators based on an eco-friendly material, thus moving the UWEH technologies towards more general applications.

4. Capacitive UWEH: Materials and designs

4.1. Silicon-on-insulator wafers

Silicon-on-insulator (SOI) wafers are an elaborately designed and manufactured multilayer semiconductor/dielectric structure (such as Si/SiO_2 (buried oxide)/Si substrate) that offers new capabilities for advanced microelectronic devices [130,131]. After more than four decades of research on materials and devices research, SOI wafers have become the mainstream of semiconductor electronics. SOI technique provides significant superiority in the design, manufacture, and performance of numerous semiconductor circuits [132,133].

Recently, a 2-degree-of-freedom (2-DOF) UWEH device was reported by Zhu et al. using a commercial SOI MEMS-based process, with a silicon device layer 25 μm and a minimized gap of 2 μm (Fig. 13a) [134]. The fabricated device composed of movable comb fingers in the *x*-*y* plane, therefore, can extract kinetic energy with arbitrary directions in the plane motion. The frequency response results verified that the designed resonance frequencies of the harvester are 38.520 and 38.725 kHz. The bandwidth was 302 Hz, which was twice broader than a comparable 1-D harvester. When the device was excited by an ultrasound transmitter for 15 s at a distance of 5 mm in the *x*-axis, a 1 μF capacitor was recharged up from 0.51 V to 0.95 V, indicating that the electricity stored on the capacitor increased by 0.321 μJ and the harvesting capability of this device was correspondingly 21.4 nW in the *x*-axis. When receiving ultrasound along the *y*-axis, the harvesting capacity was 22.7 nW.

Another improved study was reported by Fowler et al., who demonstrated a 3-DOF SOI MEMS-based ultrasound energy harvester for an implantable device (Fig. 13b) [135]. In addition to the in-plane energy harvesting principle, the device was also designed with an out-of-plane harvesting principle that enables the harvester to extract kinetic energy from ultrasound in the out-of-plane direction (*z*-axis). The out-of-plane kinetic energy of the sub-mass was extracted through a separate electrostatic sensor, which possessed the form of additional comb-shaped finger electrodes bonded on both the surrounding structure and the sub-mass. Both the out-of-plane and in-plane vibration modes are located at frequencies close to 25 kHz. Its energy harvesting capacity was demonstrated to be 24.7 nW, 19.8 nW, and 14.5 nW for the *x*, *y*, and *z*-axis, respectively. The same group also reported an omnidirectional SOI MEMS-based ultrasound energy harvester for implantable biomedical sensors and actuators (Fig. 13c) [136]. In a charging system, the harvester was rectified and stored on a capacitor with a useable voltage of about 0.6–0.9V. The maximum instantaneous electrical powers were calculated to be 49.4 nW, 35.8 nW, and 35.0 nW for the *x*, *y*, and *z*-axis, respectively.

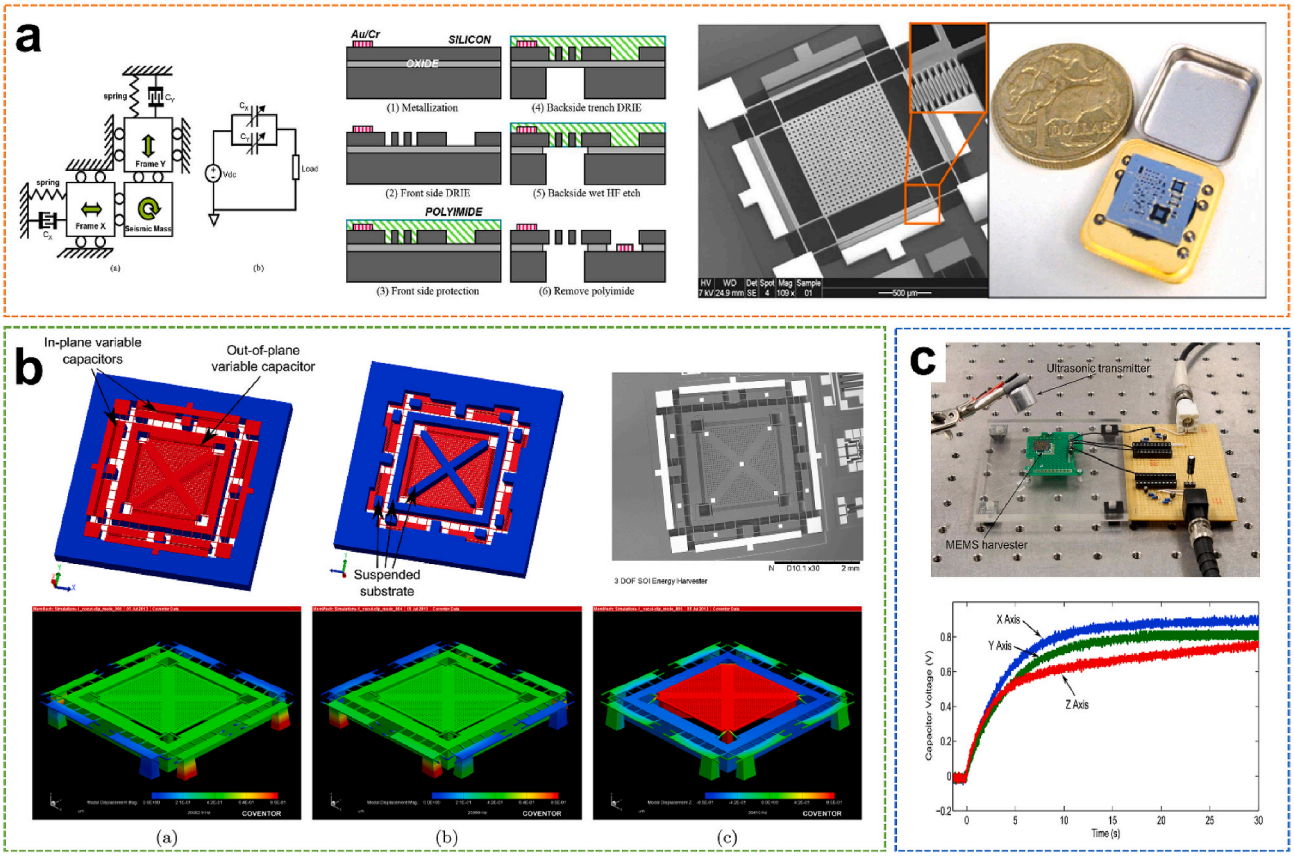

Fig. 13. SOI wafers-based UWEH. a) A 2-DOF SOI MEMS-based UWEH device. Reproduced with permission [134]. Copyright 2010, Institute of Electrical and Electronics Engineers. b) A 3-DOF SOI MEMS-based UWEH device. Reproduced with permission [135]. Copyright 2013, IOP Publishing. c) Charging performance of an omnidirectional SOI MEMS-based harvester. Reproduced with permission [136]. Copyright 2014, Institute of Electrical and Electronics Engineers.

4.2. Graphene oxide (GO) films

Graphene oxide (GO) is a derivative of graphene, consisting of hexagonal rings of carbon network possessing both sp^2-and sp^3-hybridized carbon atoms with hydroxyl and epoxide functional groups on basal planes, as well as carboxyl and carbonyl groups at the edges of the sheet [137,138]. Those functional groups can extensively modify the chemical properties and electronic structure of GO, thereby realizing numerous applications [139–141]. Moreover, the oxidation of graphite to GO will destroy the sp^2-hybrid structure, resulting in defects that extend the distance between adjacent sheets [142], consequently facilitating the delamination of GO into single-layer sheets. At present, positively charged GO films due to the capture of H^+ charges through oxygen-containing functional groups have been integrated into nanogenerators for harvesting ultrasound energy [143,144]. Que et al. reported a GO film-based flexible nanogenerator for acoustic energy harvesting (Fig. 14a) [143]. GO used to fabricate the harvester was prepared from expandable graphite flakes via the modified Hummer process [145]. The TEM image shows several layers of GO film with some folded and wrinkled regions. The dispersed GO suspensions from different concentrations and different pH solutions were then dropped onto Teflon tapes, followed by a drying process in an oven to form GO films. The diameter of the film is approximately 5.8 mm and the thickness is approximately 50 μm. In the GO film-based harvester, the charged GO film was bonded to the bottom poly(3, 4-ethylenedioxythiophene)-poly(styrenesulfonate) (PEDOT: PSS) electrode and the top was covered by the Al foil. The PEDOT: PSS electrode is grounded. When acoustic energy is transmitted, the unfixed Al membrane will respond to vibration, and the changes in capacitance would follow. This process could, therefore, yield a transient current as schematically shown. The produced current is sensitively dependent on the pH values of the suspensions used to synthesize the GO films. Harvesters prepared from suspensions of pH = 3 and pH = 5 respond strongly to acoustic vibration, producing high currents of 3.0 and 2.1

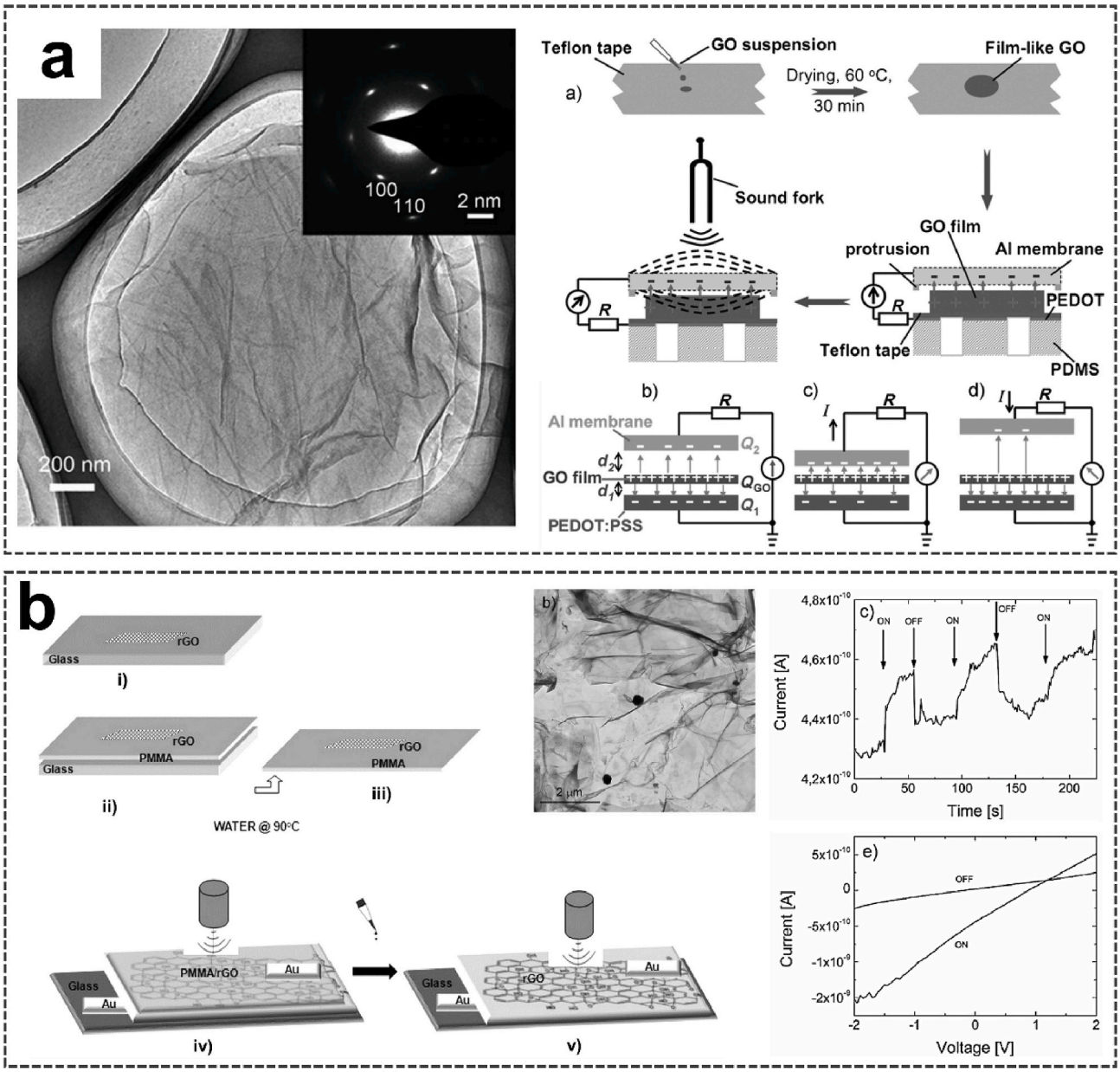

Fig. 14. GO films-based UWEH. a) Flexible UWEH device based on GO-films. Reproduced with permission [143]. Copyright 2012, Wiley-VCH. b) Poly(methyl methacrylate)/GO layered films for UWEH [144]. Copyright 2013, American Chemical Society.

nA, respectively, suggesting that the H^+ concentration actually affects the number of charges on the GO films and is essential for the current production. The conversion efficiency from acoustic energy to electricity is up to12.1%.

Another GO films-based ultrasonic nanogenerator, with a different structure based on poly(methyl methacrylate)/partially reduced GO layered films, has also been reported for ultrasound energy harvesting as shown in Fig. 14b [144]. GO films were prepared by suspension and then annealed at 400 °C for 4 h in a vacuum to obtain partially reduced GO (rGO). Poly(methyl methacrylate) (PMMA) was spin-cast onto rGO coated glass. The detached film composed of rGO flakes dispersed in the PMMA matrix was bonded to metal electrodes to form the device. The current-voltage characteristics of the prepared samples composed of pure GO and rGO films were first investigated, respectively. The partial GO deoxygenation after heat treatment improves its electrical conductivity to a certain extent. A stronger current response was also observed in the rGO sample under ultrasonic driving. The output characteristics for the PMMA/rGO harvester were then investigated. The average current of PMMA/rGO harvester is lower slightly than that of rGO ones because the electric charges in this sample are either forced to select a more circuitous route or completely confined in the narrow space inside the PMMA matrix [146]. Nevertheless, PMMA is desirable for assisting graphene-type films transfer to fabricate all the devices, which require flexible and freestanding films, because of the strong dipole interaction between chemical groups on graphene and PMMA resulting in long-chain molecules adhering to the graphene. The conversion efficiency of the PMMA/rGO nanogenerator is 19.5%. These results show a feasible strategy for fabricating UWEH devices that are easily processed, low-cost, highly efficient, freestanding, and flexible.

4.3. Organic films and pellets

Triboelectric nanogenerators have been developed since 2012 by Zhong Lin Wang [46]. It is a novel technology that can convert mechanical energy into electrical energy and has been used in many fields [147–149]. Recently, Yang et al. reported the first organic thin-film polytetrafluoroethylene (PTFE)-based triboelectric nanogenerator to harvest acoustic energy as a supportable power supply and self-powered active acoustic sensors, as shown in Fig. 15a [150]. PTFE is one of the most used materials for non-polluting and non-lubricating purposes in a dry reciprocating motion and is well known for its relevant tribological characteristics, especially low friction [151,152]. In this work, the nanogenerator is composed of a PTFE thin film and a perforated aluminum membrane electrode under delicately designed strain conditions and is able to convert acoustic energy into electricity through triboelectric transduction. The nanopores were uniformly aligned on the surface of the aluminum membrane with an average diameter of 57 ± 5 nm and a density of 210 per μm^2. The average diameter of PTFE nanowires was 54 ± 3 nm with an average length of 1.1 ± 0.4 μm. Relying on a Helmholtz cavity [151], the core of the device is in a circular shape and embedded as the flexible front plate of the cavity. The maximum power density generated is 60.2 mW m^{-2} that can light up 17 commercial LEDs simultaneously.

Analogously, PTFE-based triboelectric nanogenerator for effectively harvesting of underwater ultrasound energy was built by selecting PTFE spherical pellets as the media to perform the contact-separation operation (Fig. 15b) [32]. The device was composed of PTFE spherical pellets and two parallel Cu electrode plates bonded to an insulating cubic acrylic plate with the cylindrical holes. The device outputted an instantaneous current of approximately 100 mA and achieved a power density of 0.362 W cm^{-2} under an ultrasound frequency of 80 kHz. The calculated power conversion efficiency is as high as 13.1% with an equivalent output galvanostatic current of 1.43 mA. This nanogenerator was able to simultaneously light up to 12 lamps with 750 mW each, and drove an electronic watch, a temperature/humidity meter, and a health monitor, which demonstrated outstanding potential for underwater applications.

Another example of capacitive triboelectric technology for

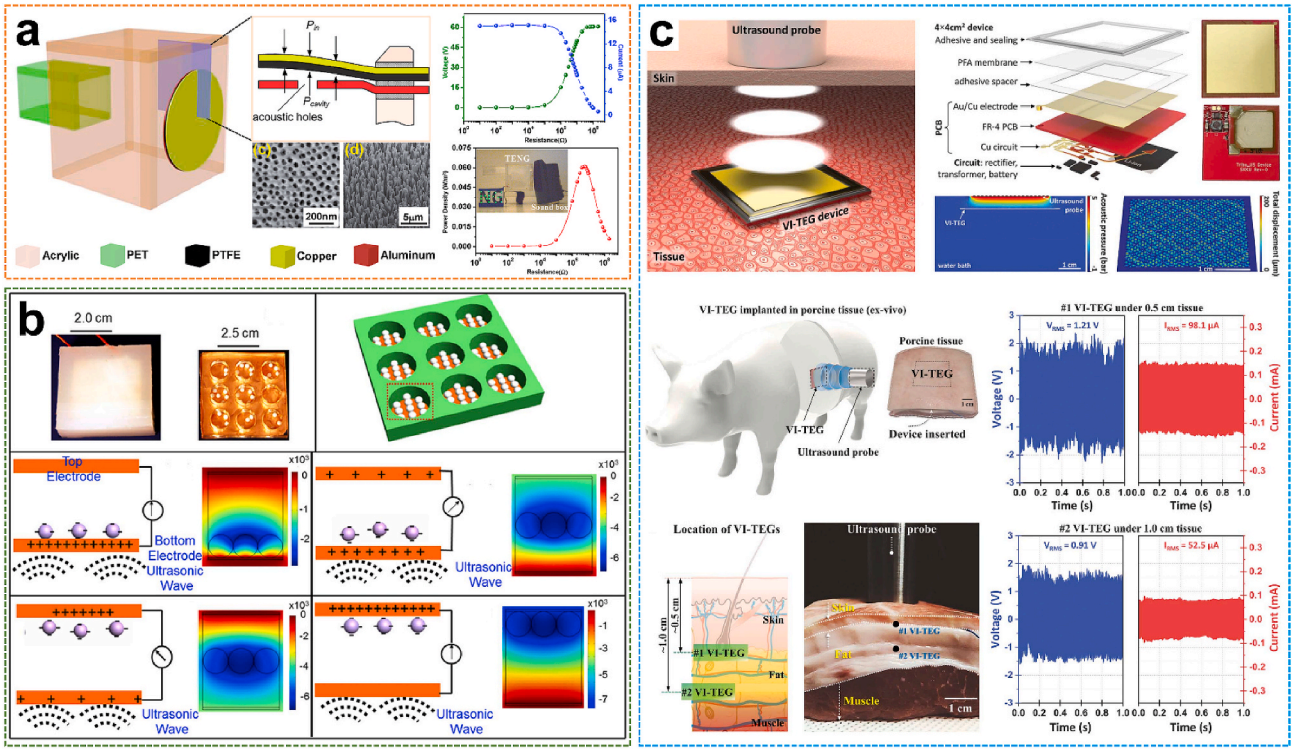

Fig. 15. Organic films and pellets-based UWEH. a) Organic thin-film PTFE-based TENG for UWEH. Reproduced with permission [150]. Copyright 2014, American Chemical Society. b) PTFE pellets-based TENG for high efficient UWEH underwater. Reproduced with permission [32]. Copyright 2017, Elsevier. c) PFA membrane-based VI-TEG for transcutaneous UWEH. Reproduced with permission [153]. Copyright 2019, American Association for the Advancement of Science.

transcutaneous ultrasound energy harvesting has been studied more recently (Fig. 15c) [153]. Using a large and thin (~50 μm thick) membrane of perfluoroalkoxy (PFA). PTA is a copolymer of tetrafluoroethylene and perfluoro ethers [154,155], with the purpose of vibrating the membrane under the pressure of ultrasound. The membrane was suspended on a thin 36 mm × 36 mm Cu electrode bonded on a flexible PCB and covered with Au. The air gap was 80 μm. The overall thickness of the vibrating and implantable triboelectric generator (VI-TEG) was less than 1 mm. This VI-TEG device realized sustainable power generating through skin and liquids. The current was increased by a factor of 1000 by using ultrasonic waves. A 0.7 mAh lithium-ion battery was recharged to 4.1 V in 4.5 h via the VI-TEG device, with an average charge rate of 166 μC s^{-1}. Finally, they performed the *ex vivo* characterizations of the VI-TEG device in an implanted environment. The VI-TEG device produced output signals of more than 98.6 mA and 1.93 V at a 10 mm distance under layered tissues including skin and fat, which are sufficient to recharge the batteries of small implants (e.g., neurostimulators or pacemakers consuming 1–100 mW) [156,157].

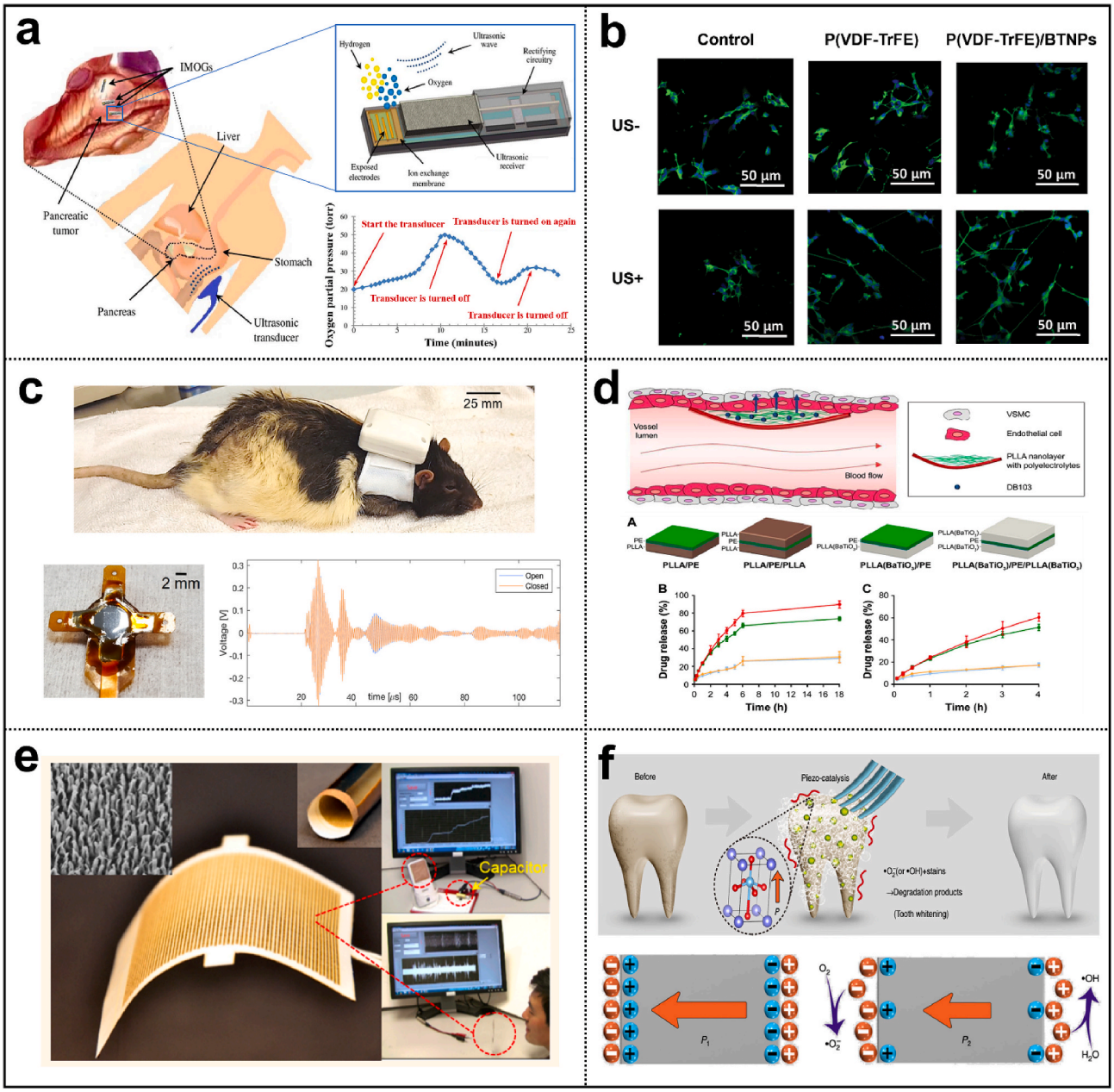

Fig. 16. Applications of UWEH. a) Wireless power for a bio-implantable device — powering an implantable micro-oxygen generator [158]. Copyright 2011, Institute of Electrical and Electronics Engineers. b) Direct cell/tissue electrical stimulations — P(VDF-TrFE)/BTNPs composite films mediate piezoelectric stimulation and promote differentiation of SH-SY5Y neuroblastoma cells [159]. Copyright 2016, Wiley-VCH. c) Wireless recording and communication in nervous systems — a wearable ultrasound system for a real-time wireless communication link with an implantable sensor mote and a remote client. Reproduced with permission [160]. Copyright 2017, Institute of Electrical and Electronics Engineers. d) Ultrasonic modulated drug delivery — nanostructured ultra-thin patches based on UWEH for the delivery of anti-restenotic drugs. Reproduced with permission [161]. Copyright 2016, Dovepress. e) Self-powered acoustic sensors — a paper-based UWEH device for self-powered sound recording. Reproduced with permission [162]. Copyright 2015, American Chemical Society. f) Ultrasound-induced piezoelectric catalysis — UWEH-based piezoelectric catalysis for nondestructive tooth whitening. Reproduced with permission [163]. Copyright 2020, Nature Publishing Group.

5. UWEH in functional applications

5.1. Progress in applications of UWEH

UWEH with different materials and device designs has been demonstrated in the previous sections. Using the UWEH technologies with the continuous optimization in structures and output performance, a series of functional applications, including wireless power for bio-implantable devices, direct cell/tissue electrical stimulations, wireless recording and communication in nervous systems, ultrasonic modulated drug delivery, self-powered acoustic sensors, and ultrasound-induced piezoelectric catalysis (Fig. 16), are generalized and discussed in this section.

5.1.1. Wireless power for bio-implantable device

Recent developments in biomedical systems, especially in micro-electronic devices for healthcare and other medical applications, illustrate the potential of bio-implantable devices. Medical implants with many benefits have become commonplace. Some possible applications are exciting and widespread, but they still require safe and reliable energy to operate. UWEH can provide a feasible route to wirelessly power these electronics *in vivo* regardless of environment conductivity or transparency.

In 2007, Zhong Lin Wang's research group first developed a UWEH-based nanogenerator that can effectively produce electricity inside biofluid (Fig. 4a and b) [57]. The output current of the nanogenerator with a 2 mm^2 size achieved as high as 35 nA. Based on the same mechanism, Donohoe et al. demonstrated powering in-body nano-sensors with ultrasound [52]. An external ultrasonic source can theoretically provide vibrational energy to implanted nanosensors that use the piezoelectric nanowires to generate power. In 2011, a UWEH powered implanted micro-oxygen generator (IMOG) has been demonstrated (Fig. 16a) [158]. *In vitro* and *ex vivo* tests showed that IMOG is capable of producing more than 150 μA which, in turn, can generate 0.525 μL min^{-1} of oxygen through electrolytic disassociation. Further, He and Shi et al. also proposed MEMS-based UWEH devices aiming at prolonging the battery lifetime of a pacemaker and other implantable medical devices (Fig. 8a,b,c) [83,87,88]. *In vitro* tests of the MEMS-based devices to transmit power through tissues showed their capability of harvesting ultrasound even from a weak intensity, and such devices can be adopted as the wireless power source for various implantable medical systems. However, the above mentioned UWEH devices are rigid and cannot be applied to curvilinear and soft surfaces. To achieve desirable flexibility to allow devices being adapted to general complex organ surfaces, our collaborators and we proposed a membrane-based flexible UWEH array (Fig. 11b) [116]. The device demonstrated flexible mechanical properties and can seamlessly adhere to curved surfaces. It also generated electricity and was successfully used to operate commercial LEDs. The voltage and current signals reached 0.9 Vpp and 2.5 μA *in vitro* test when the thickness of the placed pork tissue increased to 14 mm. Most recently, the transcutaneous UWEH using capacitive triboelectric technology reported by Hinchet et al. also demonstrated the ability to recharge small implants, such as pacemakers or neurostimulators (Fig. 15c) [153].

5.1.2. Direct cell/tissue electrical stimulations

Electrical stimulations as an artificial stimulus of neural structures have been widely applied in clinical practice and laboratory studies [164,165]. Some diseases such as Parkinson's syndromes, abnormal heart rate, and chronic pain can be relieved or cured by stimulating the brain, heart, and the spinal cord at an *in vivo* state using an electrical pulse. Compared to most biomedical stimulators that consume their assembled batteries, UWEH provides a wireless and long-term stable direct electrical stimulation strategy.

In 2010, Ciofani et al. proposed the UWEH scheme for electrically stimulating nerve cells based on piezoelectric nanoparticles (Fig. 5a) [64]. Neuronal-like PC12 cells stimulated with the UWEH strategy exhibited neurite sprout 30% higher than the control group. A non-invasive strategy for an endogenous osteoblast stimulation mediated by ultrasound-activated BNNTs was also reported by the same group [166]. They further investigated similar work using P(VDF-TrFE)/BTNPs films as substrates for neuronal stimulation, showing the applicability of ceramic/polymer composite membranes and ultrasound to neuron stimulation through the direct piezoelectric effect (Fig. 16b) [159]. In 2013, Ricotti et al. studied the effects of the combination of topographical, mechanical, chemical, and intracellular UWEH electrical stimulation on a co-culture of fibroblasts and skeletal muscle cells (Fig. 5b) [65]. The results confirmed a higher functionality of the stimulated co-cultures. Additionally, a UWEH-based approach for the inhibition of breast cancer cell proliferation was also proposed (Fig. 6c) [71], showing huge potential and versatility for the therapy of different types of cancers. In addition to directly stimulating cells, selective stimulation of peripheral nerves in the human body using UWEH implanted nanodevice has also proven to be feasible (Fig. 4c) [59]. Lately, our collaborators and we proposed a novel UWEH electrical stimulation strategy for neurodegenerative diseases, which uses direct electrical stimuli of neurons as a method to restore sight (Fig. 12) [103]. The presented stimulator can be excited by ultrasound to generate tunable outputs in an *ex vivo* test, achieving sufficient current signals (e.g., current density > 9.2 nA μm^{-2}, and current > 72 μA) for retinal stimulation. As an implantable wireless stimulator, the proposed UWEH device holds great potential in the future for retinal electrical stimulation applications.

A combination of ultrasound and nanotechnology is considered a novel strategy for wireless neural stimulations, opening exciting perspectives not only in the arena of nerve regeneration and prosthetics but also in bio-robotics and tissue engineering. Future works will focus on functionalizing nanoparticles with specific molecules in order to target them to the membranes of specific cell types. In fact, the selectivity of cell type is a fundamental aspect of performing wireless stimulation of different parts of the brain *in vivo* and fostering peculiar cellular functions.

5.1.3. Wireless recording and communication in nervous systems

Besides the powering of implantable medical devices, many applications would benefit from a bi-directional recording and communication link for control functions and data uplink. The continuous monitoring system with processing capability and able to record/communicate wirelessly could help a patient suffering from chronic diseases [167]. Traditional electrode-based methods lack the ability to record from nerves at high spatial resolution or independently from various discrete sites within a nerve bundle. Therefore, adopting new transmission technologies and miniaturizing implants into millimeter and sub-millimeter sizes can provide the possibility of possessing a network of sensor nodes in the body for applications such as multisite nerve recording, communication, and stimulation [168,169].

For example, Johnson and Seo et al. have presented ultrasonic neural dust that was constructed from low-power electronics coupled with ultrasound power delivery and backscatter communication (Fig. 10a,b,c) [20,31,106]. The extracted measurements can be reported back to the interrogator if the information is encoded in some way on the reflected ultrasonic wave through modulation. The entire system can be downsized to millimeters and has been successfully used for wireless recording and communication in cortical tissue and peripheral nervous system. Charthad et al. introduced a mm-sized implantable stimulator with ultrasound power transmission and a hybrid bi-directional data link (Fig. 10d) [107]. The implanted device fully demonstrates the capability of ultrasound power recovery and bidirectional data transmission. In addition, Piech et al. further developed a wearable (Fig. 16c) and a portable ultrasound system that establishes a real-time communication link with an implantable sensor mote and a remote client [160,170]. Future designs may integrate electrodes, biosensors, as well as

clock recovery and data modulation circuits for achieving more practical data links.

5.1.4. Ultrasonic modulated drug delivery

Drug delivery refers to an approach or process of administering a pharmaceutical compound to realize a therapeutic effect in the human body [171], which may involve scientific site-targeting within the tissue or involve facilitating systemic pharmacokinetics. For the treatment of human diseases, drug delivery is becoming increasingly important. Drug delivery is often achieved through chemical formulations of drugs, but it may also involve medical equipment or drug-device combination products [172].

For example, Vannozzi et al. reported a nanostructured ultra-thin patch for ultrasound-modulated delivery of an anti-restenotic drug (Fig. 16d) [161]. $BaTiO_3$ nanoparticles with piezoelectric properties are dispersed in the polymeric nanofilms. These devices were ultrasound-driven and able to help release anti-restenosis drugs in phosphate-buffered saline. The main mechanisms involved are the mechanical force and local potential induced by ultrasound, which enhanced polyelectrolytes disruption or poration. These results indicate that UWEH technologies can potentially serve for drug delivery, with the aim of fine control of local therapies.

5.1.5. Self-powered acoustic sensors

Ultrasonic waves, which are abundant in water and in our everyday environment, are considered to be a sustainable, clean, and ubiquitous energy source [173,174]. Therefore, harvesting acoustic energy from the ambient environment has been shown as a useful method to powering nanoelectronics or acting as a self-powered active sensor for autonomously detecting the location of a sound source [162,175]. But it is extremely challenging because of the difficulties in effectively coupling the low energy acoustic wave pulsations with the harvesting devices for energy conversion.

In 2012, Que et al. reported a flexible nano-harvester based on graphene oxide (GO) films for fork acoustic energy harvesting (Fig. 14a), with a high energy conversion efficiency of 12.1% [143]. In 2014 and 2015, Yang and Fan et al. successively reported the organic film-based and paper-based triboelectric nano-harvesters for acoustic energy harvesting and self-powered active acoustic sensing (Figs. 15a and 16e) [150]. Visualized demonstrations of the nano-harvester array for acoustic source localization have been presented. In 2017, Xi et al. proposed high efficient harvesting of underwater ultrasound triboelectric technology (Fig. 15b) [32]. The presented device can be used in both shallow and deep water. Most recently, a PVDF nanofibers-based nanogenerator for acoustic energy harvesting and self-powered multifunctional sensing was also reported [176]. Therefore, the concept and design based on UWEH technologies can be further utilized in various situations for either energy-harvesting or environment-sensing purposes, such as sensor networks, infrastructure monitoring, acoustic source localization, and environmental noise reduction.

5.1.6. Ultrasound-induced piezoelectric catalysis

Piezoelectric materials have spontaneous polarization potential, which can be adjusted by applying stress on the materials due to the piezoelectric effect [177]. Analogous to photocatalysis, where the photo-induced electric charges (electron-hole pairs) participate in the catalytic redox reactions, in theory, piezoelectric charges (positive and negative ones) induced by mechanical vibration can also be applied to drive catalytic redox reactions, which can be called as piezocatalysis [77].

Several investigations have proved the concept that ultrasound can be utilized as irradiation energy to improve piezocatalysis. For example, in 2015, Li et al. reported an enhanced $BaTiO_3$ nanocrystals-based hybrid photocatalysis by ultrasound-induced piezo-phototronic effect [178]. $BaTiO_3$ nanocrystals in responding to ultrasound act as an alternating built-in electric field to separate photoinduced carriers consecutively, effectively enhancing the photocatalytic activity. Further, Su et al. realized improved H_2 evolution based on UWEH-assisted piezocatalysis of modified MoS_2 [78]. A high H_2 evolution of ~1250 μmol g^{-1} h^{-1} was achieved. You et al. also demonstrated the powerful effects of UWEH in piezocatalytic hydrogen production and dye decomposition based on BiFeO3 nanosheets (Fig. 7) [34]. In addition, Feng et al. first proposed the application of ultrasound-induced piezoelectric catalysis for disinfection [33]. It has been found that there is a significant improvement in ultrasonic inactivation of *E. coli* by using the piezoelectric effect. In addition to the applications mentioned above, ultrasound-induced piezoelectric catalysis can also be applied for nondestructive tooth whitening and tumor therapy [163,179]. For example, Wang et al. demonstrated the biocompatible, cost-effective, time-efficient and nondestructive tooth whitening scheme via ultrasound-driven $BaTiO_3$ nanoparticles for simulating daily brushing (Fig. 16f) [163]. The work showed the potential of ultrasound-induced piezoelectric catalysis to be developed into a green technology widely used in the home. Recently, Zhu et al. proposed and demonstrated a high efficiency piezocatalytic therapy modality for tumors based on the reactive oxygen species generation by the ultrasound-induced piezoelectric response [179], which provides a novel and promising strategy for the non-invasive flank tumor therapy by nanocatalytic medicine and is of great significance for the future potential clinical translation.

5.2. Design considerations of biomedical UWEH systems

To better understand the applications of UWEH, we composed the statistics on the percentage of publications in 2007–2020 related to the UWEH technologies (Fig. 17a). It can clearly show the demand of wireless power for biomedical related UWEH systems received more attention due to continuous advances in biotechnologies and micro/nano device designs, which minimize the power required for implantable bioelectronics. The average power consumption and voltage inputs of representative implantable bioelectronic products are listed in Table 1. Biosensing systems typically consume lower power ($<\approx$ 50 μW), and the main consumption may come from communication, analog-to-digital conversion or signal amplification and processing [180–182]. Radio frequency (RF) data transmission requires approximately 10 μW to 1.5 mW [183,184]. In contrast, the energy required for stimulation spans a broad range, for example, 5–100 μW for pacemakers [185,186], and 4.5–21 mW for muscle stimulation [187]. UWEH technologies have shown sufficient, stable, reliable, and safe output that can be used in a broad range of applications.

Further research into materials and device designs that integrate various strategies may potentially realize innovative solutions of miniaturized biocompatible power systems to meet the operating characteristics demanded by a wide range of bio-implantable electronic devices. However, a primary design strategy for any energy harvesting system is to minimize energy losses. The main power losses for an UWEH-based implant are caused by acoustic beam divergence, acoustic absorption, acoustic reflection, acoustic-electric conversion, power electronics, and load impedance mismatch [89]. A schematic diagram of these losses is shown in Fig. 17b. In this section, a brief discussion of each loss and other considerations is demonstrated in order to better optimize the UWEH system for implantable applications.

5.2.1. Beam divergence

Acoustic beam divergence depends largely on the geometry design of the ultrasound transmitter, i.e. the ratio of the transmitter diameter to the ultrasonic wavelength. For an unfocused circular plate transmitter, the beam radius (r_{beam}) is described with Formula (1) and the corresponding ultrasonic power diverted is described with Formula (2) [89]:

$$r_{beam} \approx \begin{cases} \text{Near Field} \rightarrow a \\ \text{Far Field} \rightarrow d \cdot \tan\left(\sin^{-1}\left(\frac{0.61c}{af}\right)\right) \end{cases}, \quad (1)$$

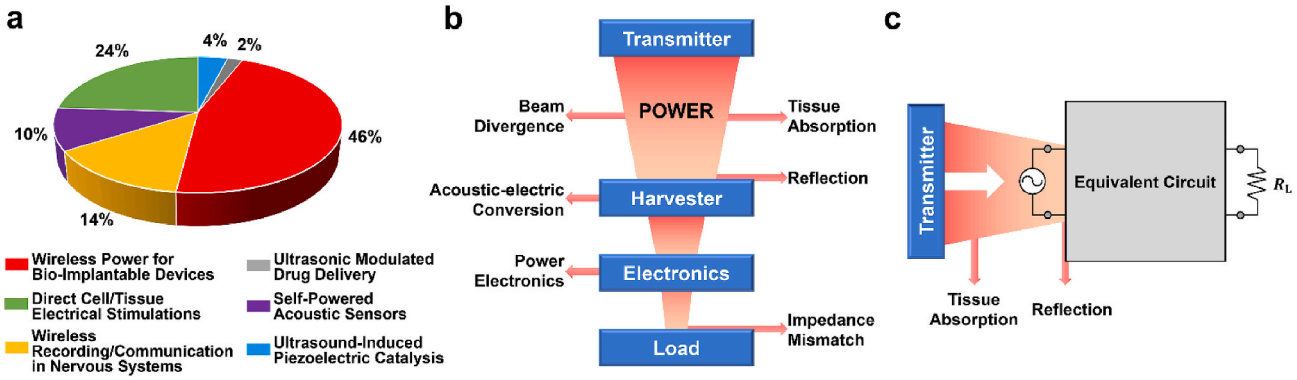

Fig. 17. Application statistics and design analysis of power losses in implantable UWEH systems. a) Publications on UWEH technologies with applications for wireless power for bio-implantable devices, direct cell/tissue electrical stimulations, wireless recording and communication in nervous systems, ultrasonic modulated drug delivery, self-powered acoustic sensors, and ultrasound-induced piezoelectric catalysis in refereed journals in the time period of 2007–2020. b) Schematic of power losses in an implantable UWEH system. c) Circuit model of an implantable UWEH system (inspired from Ref. [89]).

Table 1
Requirements of voltage inputs and power consumptions for various bioelectronics.

Representative bioelectronics		Voltage inputs	Power consumptions	Refs
Biosensors	Timers for biosensors	0.3–1.3 V	<660 pW	[188, 189]
	Analogue-to-digital conversion	1.2–1.5 V	<35 μW	[180, 181]
Communications	Radiofrequency transmitters	0.5–1.2 V	10 μW to 1.5 mW	[183, 184]
	Ultrasonic transmitters	0.5–2.0 V	0.5–1.5 mW	[190, 191]
Stimulations	Electrical stimulations	1.6–3 V	1 μW to 25 mW	[153, 185, 192, 193]
	Actuators	4–4.5 V	50–100 mW	[182, 194]

$$\frac{P_{\text{diverted}}}{P_{\text{transmitter face}}} = 1 - \frac{a^2}{r_{\text{beam}}^2}, \tag{2}$$

wherein a is the diameter of the piezoelectric material in the transmitter, d is the depth of penetration, c is the acoustic velocity, and f is the ultrasonic frequency. Therefore, for miniaturized energy harvesting systems, energy harvesting efficiency can be improved by focusing the ultrasound beam. Additionally, high-frequency ultrasound possesses a shorter wavelength that can produce an excellent spatial resolution by focusing the power on the size of a millimeter and even smaller point.

5.2.2. Tissue absorption

The acoustic power absorbed in tissue, or tissue heating, is heavily dependent on ultrasonic frequency, which is given in Formula (3) [195]:

$$\frac{P_{\text{absorbed}}}{P_{\text{source}}} = 1 - e^{-2\alpha_0 f^n d}, \tag{3}$$

wherein d is the penetration depth, and α_0 is the frequency-dependent acoustic absorption coefficient. As the acoustic frequency increases linearly, the remaining ultrasound energy decreases exponentially after passing through the medium. Hence, a low-frequency ultrasound should be selected as the energy source in order to minimize power losses caused by absorption.

5.2.3. Acoustic interface and reflection

Acoustic interface refers to the boundary between two materials with different acoustic impedances [196]. When acoustic waves enter an acoustic interface with normal incidence, a certain amount of ultrasound energy is transmitted across the interface and a certain amount of energy is reflected. Reflection of ultrasound off the surface of the implanted device is because of the acoustic impedance mismatch between the tissue and the implant. The power reflected is given in Formula (4) [195]:

$$\frac{P_{\text{reflected}}}{P_{\text{generator face}}} = \left(\frac{Z_i - Z_t}{Z_i + Z_t}\right)^2, \tag{4}$$

wherein Z_i and Z_t are the acoustic impedance of the implant and tissue, respectively. For example, the acoustic impedances of piezoelectric ceramics and crystals are generally large (20–30 MRayls), but the acoustic impedance of the tissue is relatively low (~1.5 MRayls). An effective way to lower the reflection is to bond an acoustic matching layer onto the piezoelectric layer of the harvester. Ideal acoustic impedances of the matching layer (Z_{ml}) can be calculated by Formula (5) as follows [177]:

$$Z_{\text{ml}} = (Z_i Z_t)^{1/2}. \tag{5}$$

Additionally, constructing a 1–3 piezoelectric composite consisted of piezoelectric arrays and a non-piezoelectric inactive polymer can effectively reduce the acoustic impedance, thereby reducing the energy loss caused by acoustic reflection.

5.2.4. Acoustic-electric conversion

Improving energy conversion efficiency is the primary consideration of any harvesters, which depends primarily on the material selected. For instance, the anisotropic 1–3 piezo-composites, which combine the desirable properties of two different phases, exhibit superior coupling characteristics than the isotropic piezoelectric structures in ultrasound energy harvesting applications [113,197]. This strategy proved to be feasible in designing 1–3 type piezo-composite consisted of the piezoelectric arrays and non-piezoelectric polymer [27,110,198]. The vibration for each piezoelectric pillar is dominant in the basic longitudinal 3-3 direction with a higher efficiency determined by the electromechanical coupling coefficient k_{33}. Although pure ceramic or single crystal disk exhibits a high piezoelectric constant d_{33}, the piezoelectric voltage factor g_{33} ($= d_{33}/\varepsilon_{33}$) is relatively low because of the high dielectric constant. Therefore, a pure piezoceramic or single crystal layer is not a better receiver for the ultrasound. The scheme of piezo-composite configuration inspired researchers to develop a 1–3 piezoelectricity/polymer structure to enhance the k_{33} and g_{33} factors, thereby optimizing the sensitivity in the acoustic receiving mode. At present, the development of 3D printing technology has facilitated the design of a series of complex composite structures [199–202]. If the receiving sensitivity is enhanced, the human body can be interrogated at lower ultrasonic power and the ultrasonic biological effect will be minimized.

5.2.5. Power electronics and electrical matching

In order to be compatible with sensors or other electronics, power electronics are required to regulate the power whether they are passive or active. The alternating current (AC) peaks produced by the ultrasound harvesters are not applicable to the direct current (DC) system of general electronic devices. Therefore, the AC output needs to be rectified into a common DC output through a rectifier circuit. The output voltage amplitude and power are a function of the load resistance R_L. The electrical impedance mismatch is analogous to acoustic impedance mismatch, where the electricity is reflected instead of ultrasound, and the mismatch is between the electrical impedance of the material and the load impedance. Within ultrasound devices, electrical matching is often referred to as tuning. For example, tuning a piezoelectric harvester requires attaching a resistor and an inductor in parallel with the capacitance (C_0) to match the mechanical resonance (ω) with the electrical resonance. Tuning can be performed to significantly increase the generated power. Nevertheless, it may not be feasible to match the desirable resistor and inductor on an implantable device because it usually depends on the dimension and mechanical resonance frequency of the harvester. Thus, complete complex matching (inductor and resistor) could be replaced by single resistance matching ($R_L = 1/\omega C_0$), shown in Fig. 17c, for simplification.

5.2.6. Other considerations

In addition to reducing the above losses, there are other factors worth considering for biomedical UWEH systems, such as biocompatibility, mechanical compliance, and safety. After a device is implanted into the human body, it has an impact and effect on the surrounding biological tissue environment [203]. Thus, the biocompatibility of the materials is an important indicator to be considered and evaluated when considering their applications in medicine. The material is not only required to have very low toxicity [204], but also be able to properly stimulate the corresponding function of the body in specific applications. Additionally, the surfaces of tissues or organs in the body, such as intestine, blood vessels, and heart, are always complex, which require devices with desirable flexibility to make them be suitable for general concave-convex surfaces. To address the challenge, flexible and stretchable electronics will be the direction of future development [198,205–207]. At last, the intensity of ultrasound must be kept within a safe medical range. Although ultrasonic diagnosis and therapeutics have long been used in medical, according to FDA standards, only a limited ultrasound intensity of 720 mW cm^{-2} is permitted to enter the human body [28,208].

6. Conclusions and outlook

This review summarizes some recent advances in the field of ultrasound-induced wireless energy harvesting technologies that have been used in a series of studies and applications, including wireless power for bio-implantable devices, direct cell/tissue electrical stimulations, wireless recording and communication in nervous systems, ultrasonic modulated drug delivery, self-powered acoustic sensors, and ultrasound-induced piezoelectric catalysis. As explained in this review, UWEH could be divided into two major categories: piezoelectric energy harvesting — which includes piezoelectric nanomaterials-based, piezoelectric films/diaphragms-based, and piezoelectric ceramics and composites-based systems, and capacitive energy harvesting — which includes electret-based electrostatic and triboelectric systems. Fig. 18 gives a summary of the development of UWEH since 2007. Since the influential publication of the UWEH by Zhong Lin Wang's group, researchers around the world, including the United States, China, Italy, South Korea, etc., are focusing on this field. Advances in nanotechnologies, microelectronics, and biomedical systems are revolutionizing UWEH. Their synergy can be greatly powerful and can play a vital role in a range of emerging applications. UWEH technologies from the perspective of material strategies, fabrication techniques, design considerations, and function applications have been discussed systematically. UWEH technologies have definitely shown a stable, reliable, and safe output for a wide range of applications.

The future development UWEH will be contributed by the following aspects (Fig. 19): (1) Firstly, the development of novel materials with high energy harvesting capability. Currently, the piezoelectric materials are limited to traditional ZnO, PZT, $BaTiO_3$, and PVDF, etc. Novel materials with high and new performance (e.g., acoustic, electrical, and mechanical characteristics) and new structures, such as piezoelectric metamaterials [210], and biomimetic structures [211], are on demand to increase the energy harvesting efficiency and prolong the lifetime of the energy harvesting device. Besides, with the development of bio-implantable UWEH devices, new materials with non-toxic, biocompatible and even biodegradable properties are on demand for next-generation energy harvesting devices. (2) Second, for the development of the UWEH devices, the novel fabrication technology and structural design will be on demand for the applications on special surfaces or circumvent. For example, 3D and 4D printing have been widely used in the customized design to fabricate smart structures and has facilitated the fabrication of miniaturized and complex piezoelectric ceramic structures to achieve desirable performance and even time-dependent deformations [200,212–215]. The direct ink writing (DIW)-based 3D printing of polymer-based piezoelectric structures has been widely studied [216,217]. Novel fabrication technology, such as controlling the alignment of nanofibers during 3D printing, needs to be developed to achieve high performance of energy harvesting. For the structural design, the applications on curved surfaces need the development of devices with high stretchability and long lifetime. Currently, the stretchable UWEH devices made with piezoelectric polymers have the disadvantage of low performance, while the ceramic-based stretchable UWEH devices have the demerit of low stretchability. New devices integrated with self-healing capability can benefit from

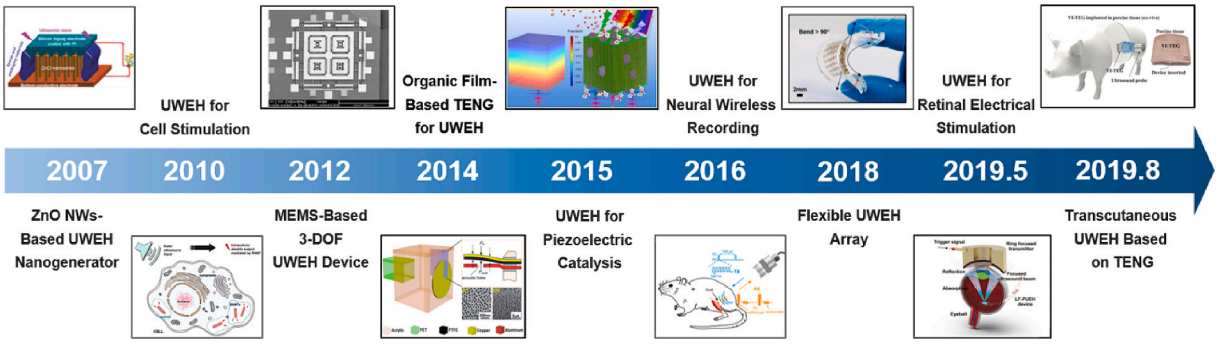

Fig. 18. A summary of the development of UWEH since 2007. Reproduced with permissions [20,30,64,103,116,150,153,178,209]. Copyright 2007, 2019, American Association for the Advancement of Science. Copyright 2010, 2014, 2015, American Chemical Society. Copyright 2012, Institute of Electrical and Electronics Engineers. Copyright 2016, 2018, Elsevier. Copyright 2019, Wiley-VCH.

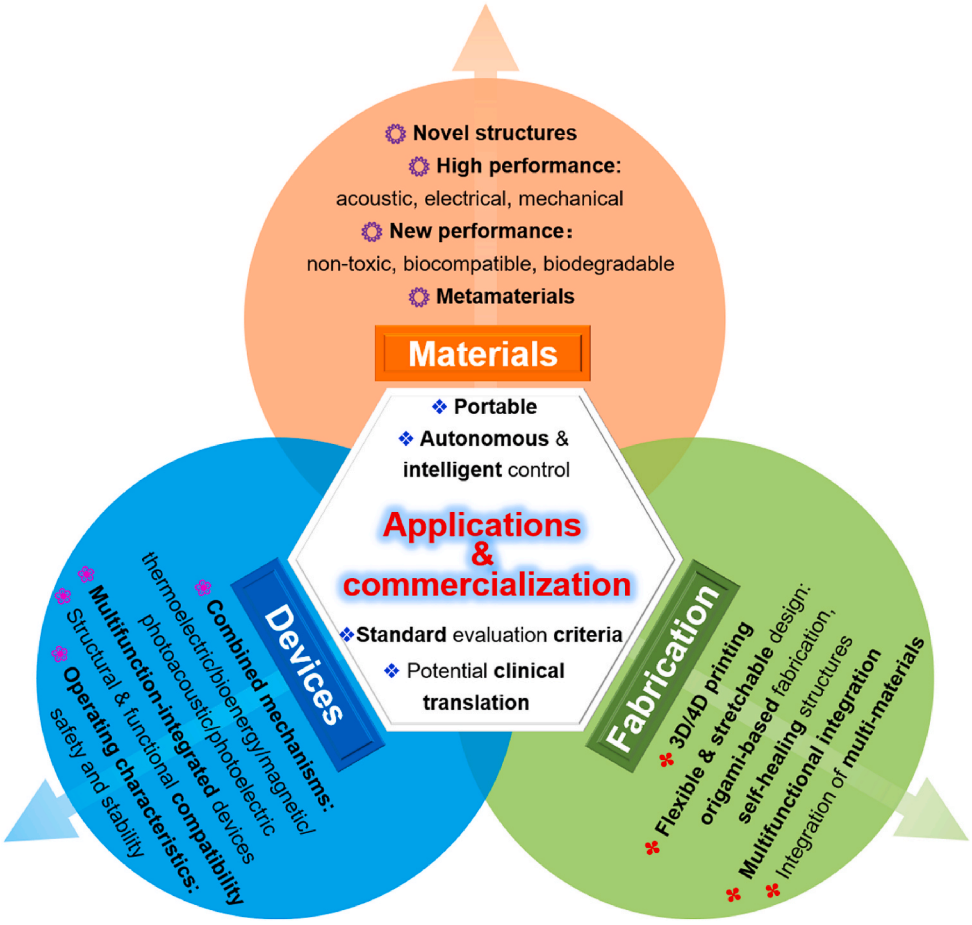

Fig. 19. Perspectives on the future development of UWEH technology.

long-term use as well as improved maintenance, reliability, and durability. Also, UWEH devices require a special angle related to the ultrasonic wave to achieve the optimal performance. Current UWEH devices will require a long time to find a favorable angle, and a new design to achieve the best performance at arbitrary angles need to be developed. Furthermore, some of the bio-implantable devices require shape changing after implantation. The origami-based UWEH devices may be suitable for such applications, which are small and easy to implant and will change its geometry to realize high performance after implantation. Some bioinspired designs will be interesting and may guide the designs of UWEH devices to achieve high performance. (3) For the applications of UWEH, currently, it is limited to piezoelectric/capacitive devices. New energy harvesting mechanisms or the novel combination of current energy harvesting mechanisms such as thermoelectric/magnetic/bioenergy/photoacoustic/photoelectric need to be developed to enhance the efficiency. For example, during the application of an ultrasound wave on the UWEH device, lots of the energy is dissipated through heat and hence wasted. The combination of UWEH device with the thermoelectric device will transfer the waste heat to energy and significantly increase the efficiency. Other applications besides energy harvesting also need to be developed to broaden the applications of UWEH. For example, the ultrasound-induced energy generation will trigger the piezoelectric behavior, and the current generated will enhance the healing efficiency of the bone structure made with the combination of hydroxyapatite-tricalcium phosphate (HATCP) and piezoelectric nanoparticles (e.g., $BaTiO_3$, KNN, $BiFeO_3$). The stimulation by ultrasound will also increase the cell growth speed by using a piezoelectric scaffold. Additionally, ultrasound-induced piezocatalytic therapeutic modality that integrates ultrasound, piezocatalysis, and tumor therapy together will provide a novel and promising strategy for the non-invasive flank tumor therapy by nanocatalytic medicine, which is of great significance for the future potential clinical translation.

All in all, we hope this work can provide a summary of current UWEH developments for further study and inspire better design of UWEH technology and other wireless electronics and systems. Portable, high-performance, autonomous, and even biodegradable electronics and nano/micro bio-robotics combined with UWEH are the next-generation smart devices that are rapidly developing. A befitting energy transfer strategy that is structurally and functionally compatible with these systems is extremely important. The integration of these features can broaden their practical functions, especially for medical devices that need to be implanted in the human body. Additionally, standard evaluation criteria are also necessary for qualitative and quantitative evaluation of the UWEH device performance, as well as their potential for practical applications and commercialization. Future studies in this field will also focus on the intelligent and autonomous control of their dynamic properties, such as the dynamic transfer efficiency, operational safety and stability, as well as other ultrasound-induced effects.

Declaration of competing interest

The authors declare no conflict of interest.

Acknowledgements

This work was partially supported by the National Institutes of Health (NIH) under grant 1R01EY026091, R01 EY028662 and R01 HL127271, National Science Foundatio (NSF) CMMI 1663663, and an UNRESTRICTED GRANT to the Department of Ophthalmology at USC

from Research to Prevent Blindness, New York, NY.

References

[1] A. Yakovlev, S. Kim, A. Poon, IEEE Commun. Mag. 50 (2012) 152–159.
[2] B. Shi, Z. Li, Y. Fan, Adv. Mater. 30 (2018) 1801511.
[3] S. Bhunia, S. Majerus, M. Sawan, Implantable Biomedical Microsystems: Design Principles and Applications, Elsevier, 2015.
[4] K. Bazaka, M.V. Jacob, Electronics 2 (2013) 1–34.
[5] G.T. Hwang, M. Byun, C.K. Jeong, K.J. Lee, Adv. Healthc. Mater. 4 (2015) 646–658.
[6] B.C. Kim, J.Y. Hong, G.G. Wallace, H.S. Park, Adv. Energy Mater. 5 (2015) 1500959.
[7] M. Li, J. Lu, Z. Chen, K. Amine, Adv. Mater. 30 (2018) 1800561.
[8] F.M. Merchant, T. Quest, A.R. Leon, M.F. El-Chami, J. Am. Coll. Cardiol. 67 (2016) 435–444.
[9] C. Pan, Z. Li, W. Guo, J. Zhu, Z.L. Wang, Angew. Chem. Int. Ed. 50 (2011) 11192–11196.
[10] S.K. Ghosh, P. Adhikary, S. Jana, A. Biswas, V. Sencadas, S.D. Gupta, B. Tudu, D. Mandal, Nano Energy 36 (2017) 166–175.
[11] I. Jeerapan, J.R. Sempionatto, J. Wang, Adv. Funct. Mater. (2019) 1906243.
[12] Y. Lu, J. Chen, Z. Cheng, S. Zhang, Energy Convers. Manag. 200 (2019) 112084.
[13] Y. Sun, J. Chen, X. Li, Y. Lu, S. Zhang, Z. Cheng, Nano Energy 61 (2019) 337–345.
[14] Y. Bai, H. Jantunen, J. Juuti, Adv. Mater. 30 (2018) 1707271.
[15] K. Agarwal, R. Jegadeesan, Y.-X. Guo, N.V. Thakor, IEEE Rev. Biomed. Eng. 10 (2017) 136–161.
[16] H. Peng, L. Mao, X. Qian, X. Lu, L. Jiang, Y. Sun, Q. Zhou, IEEE Trans. Ultrason. Ferroelectrics Freq. Contr. 67 (2019) 735–744.
[17] S. Ha, C. Kim, P.P. Mercier, G. Cauwenberghs, High-density Integrated Electrocortical Neural Interfaces: Low-Noise Low-Power System-On-Chip Design Methodology, Academic Press, 2019.
[18] E. MacDonald, R. Wicker, Science 353 (2016) aaf2093.
[19] H. Basaeri, D.B. Christensen, S. Roundy, Smart Mater. Struct. 25 (2016) 123001.
[20] D. Seo, R.M. Neely, K. Shen, U. Singhal, E. Alon, J.M. Rabaey, J.M. Carmena, M. M. Maharbiz, Neuron 91 (2016) 529–539.
[21] A.Y. Cheung, A. Neyzari, Canc. Res. 44 (1984) 4736s–4744s.
[22] P. Gélat, G. Ter Haar, N. Saffari, Phys. Med. Biol. 57 (2012) 8471.
[23] M.D. Menz, Ö. Oralkan, P.T. Khuri-Yakub, S.A. Baccus, J. Neurosci. 33 (2013) 4550–4560.
[24] K.G. Baker, V.J. Robertson, F.A. Duck, Phys. Ther. 81 (2001) 1351–1358.
[25] D.L. Miller, N.B. Smith, M.R. Bailey, G.J. Czarnota, K. Hynynen, I.R.S. Makin, Bioeffects Committee of the American Institute of Ultrasound in Medicine, J. Ultrasound Med. 31 (2012) 623–634.
[26] J. Provost, C. Papadacci, J.E. Arango, M. Imbault, M. Fink, J.-L. Gennisson, M. Tanter, M. Pernot, Phys. Med. Biol. 59 (2014) L1.
[27] L. Jiang, R. Chen, J. Xing, G. Lu, R. Li, Y. Jiang, K.K. Shung, J. Zhu, Q. Zhou, J. Appl. Phys. 125 (2019) 214501.
[28] W.F. Pritchard Jr., R.F. Carey, Radiology 205 (1997) 27–36.
[29] J.C. Lin, IEEE Antenn. Propag. Mag. 48 (2006) 157–159.
[30] X. Wang, J. Song, J. Liu, Z.L. Wang, Science 316 (2007) 102–105.
[31] B.C. Johnson, K. Shen, D. Piech, M.M. Ghanbari, K.Y. Li, R. Neely, J.M. Carmena, M.M. Maharbiz, R. Muller, in: IEEE Custom Integrated Circuits Conference (CICC), IEEE 2018, 2018, pp. 1–4.
[32] Y. Xi, J. Wang, Y. Zi, X. Li, C. Han, X. Cao, C. Hu, Z. Wang, Nano Energy 38 (2017) 101–108.
[33] J. Feng, Y. Fu, X. Liu, S. Tian, S. Lan, Y. Xiong, ACS Sustain. Chem. Eng. 6 (2018) 6032–6041.
[34] H. You, Z. Wu, L. Zhang, Y. Ying, Y. Liu, L. Fei, X. Chen, Y. Jia, Y. Wang, F. Wang, Angew. Chem. Int. Ed. 58 (2019) 11779–11784.
[35] T.G. Leighton, Prog. Biophys. Mol. Biol. 93 (2007) 3–83.
[36] S. Chandrasekaran, C. Bowen, J. Roscow, Y. Zhang, D.K. Dang, E.J. Kim, R. Misra, L. Deng, J.S. Chung, S.H. Hur, Phys. Rep. 792 (2019) 1–33.
[37] Z. Gao, J. Zhou, Y. Gu, P. Fei, Y. Hao, G. Bao, Z.L. Wang, J. Appl. Phys. 105 (2009) 113707.
[38] Q. Zheng, B. Shi, Z. Li, Z.L. Wang, Adv. Sci. 4 (2017) 1700029.
[39] E.O. Torres, G.A. Rincón-Mora, IEEE Trans. Circ. Syst. I: Regul. Pap. 56 (2008) 1938–1948.
[40] Y. Chiu, V.F. Tseng, J. Micromech. Microeng. 18 (2008) 104004.
[41] Y. Zhang, A. Luo, Y. Xu, T. Wang, A. Zhang, F. Wang, in: 12th IEEE/ASME International Conference on Mechatronic and Embedded Systems and Applications (MESA), IEEE 2016, 2016, pp. 1–6.
[42] Y. Suzuki, IEEJ Trans. Electr. Electron. Eng. 6 (2011) 101–111.
[43] Y. Fei, Z. Xu, C. Chen, in: Proceedings. IEEE SoutheastCon 2001 (Cat. No. 01CH37208), IEEE, 2001, pp. 1–7.
[44] S. Boisseau, G. Despesse, B.A. Seddik, Small-Scale Energy Harvesting, 2012, pp. 1–39.
[45] C. Wu, A.C. Wang, W. Ding, H. Guo, Z.L. Wang, Adv. Energy Mater. 9 (2019) 1802906.
[46] F.-R. Fan, Z.-Q. Tian, Z.L. Wang, Nano Energy 1 (2012) 328–334.
[47] H. Ouyang, Z. Li, Sci. Bull. 64 (2019) 1565–1566.
[48] K. Jenkins, R. Yang, Piezoelectric Nanomaterials for Energy Harvesting, Nanomaterials for Sustainable Energy, Springer, 2016, pp. 193–213.
[49] L. Vayssieres, Adv. Mater. 15 (2003) 464–466.
[50] R. Agrawal, B. Peng, E.E. Gdoutos, H.D. Espinosa, Nano Lett. 8 (2008) 3668–3674.
[51] Z.L. Wang, Mater. Sci. Eng. R Rep. 64 (2009) 33–71.
[52] M. Donohoe, S. Balasubramaniam, B. Jennings, J.M. Jornet, IEEE Trans. Nanotechnol. 15 (2015) 151–154.
[53] F. Mazzilli, P.E. Thoppay, V. Praplan, C. Dehollain, in: 2012 IEEE International Symposium on Circuits and Systems, IEEE, 2012, pp. 2865–2868.
[54] Z.L. Wang, J. Song, Science 312 (2006) 242–246.
[55] X. Liu, L. Gu, Q. Zhang, J. Wu, Y. Long, Z. Fan, Nat. Commun. 5 (2014) 1–9.
[56] S. Xu, Y. Qin, C. Xu, Y. Wei, R. Yang, Z.L. Wang, Nat. Nanotechnol. 5 (2010) 366.
[57] X. Wang, J. Liu, J. Song, Z.L. Wang, Nano Lett. 7 (2007) 2475–2479.
[58] X. Wang, Y. Gao, Y. Wei, Z.L. Wang, Nano Res. 2 (2009) 177–182.
[59] M. Donohoe, B. Jennings, J.M. Jornet, S. Balasubramaniam, IEEE Trans. Nanotechnol. 16 (2017) 919–930.
[60] D. Golberg, Y. Bando, C. Tang, C. Zhi, Adv. Mater. 19 (2007) 2413–2432.
[61] J.H. Kang, G. Sauti, C. Park, V.I. Yamakov, K.E. Wise, S.E. Lowther, C.C. Fay, S. A. Thibeault, R.G. Bryant, ACS Nano 9 (2015) 11942–11950.
[62] J. Qi, X. Qian, L. Qi, J. Feng, D. Shi, J. Li, Nano Lett. 12 (2012) 1224–1228.
[63] G. Ciofani, A. Menciassi, Piezoelectric Nanomaterials for Biomedical Applications, Springer, 2012.
[64] G. Ciofani, S. Danti, D. D'Alessandro, L. Ricotti, S. Moscato, G. Bertoni, A. Falqui, S. Berrettini, M. Petrini, V. Mattoli, ACS Nano 4 (2010) 6267–6277.
[65] L. Ricotti, T. Fujie, H. Vazao, G. Ciofani, R. Marotta, R. Brescia, C. Filippeschi, I. Corradini, M. Matteoli, V. Mattoli, PloS One 8 (2013).
[66] A. Koppes, K. Keating, A. McGregor, R. Koppes, K. Kearns, A. Ziemba, C. McKay, J. Zuidema, C. Rivet, R. Gilbert, Acta Biomater. 39 (2016) 34–43.
[67] Y.-S. Lee, G. Collins, T.L. Arinzeh, Acta Biomater. 7 (2011) 3877–3886.
[68] C.E. Schmidt, V.R. Shastri, J.P. Vacanti, R. Langer, Proc. Natl. Acad. Sci. Unit. States Am. 94 (1997) 8948–8953.
[69] A.H. Rajabi, M. Jaffe, T.L. Arinzeh, Acta Biomater. 24 (2015) 12–23.
[70] A. Marino, S. Arai, Y. Hou, E. Sinibaldi, M. Pellegrino, Y.-T. Chang, B. Mazzolai, V. Mattoli, M. Suzuki, G. Ciofani, ACS Nano 9 (2015) 7678–7689.
[71] A. Marino, M. Battaglini, D. De Pasquale, A. Degl'Innocenti, G. Ciofani, Sci. Rep. 8 (2018) 1–13.
[72] S. Basu, L. Martin, Y. Chu, M. Gajek, R. Ramesh, R. Rai, X. Xu, J. Musfeldt, Appl. Phys. Lett. 92 (2008), 091905.
[73] T. Choi, S. Lee, Y.J. Choi, V. Kiryukhin, S.-W. Cheong, Science 324 (2009) 63–66.
[74] T. Gao, Z. Chen, Q. Huang, F. Niu, X. Huang, L. Qin, Y. Huang, Rev. Adv. Mater. Sci. 40 (2015) 97–109.
[75] J.M. Park, S. Nakashima, M. Sohgawa, T. Kanashima, M. Okuyama, Jpn. J. Appl. Phys. 51 (2012), 09MD05.
[76] S. Singh, H. Ishiwara, K. Maruyama, Appl. Phys. Lett. 88 (2006) 262908.
[77] Y. Feng, L. Ling, Y. Wang, Z. Xu, F. Cao, H. Li, Z. Bian, Nano Energy 40 (2017) 481–486.
[78] Y. Su, L. Zhang, W. Wang, X. Li, Y. Zhang, D. Shao, J. Mater. Chem. 6 (2018) 11909–11915.
[79] Z. Huang, Y. Hao, Y. Li, H. Hu, C. Wang, A. Nomoto, T. Pan, Y. Gu, Y. Chen, T. Zhang, Nat. Electron. 1 (2018) 473–480.
[80] M.M. Shulaker, G. Hills, R.S. Park, R.T. Howe, K. Saraswat, H.-S.P. Wong, S. Mitra, Nature 547 (2017) 74–78.
[81] K.I. Park, J.H. Son, G.T. Hwang, C.K. Jeong, J. Ryu, M. Koo, I. Choi, S.H. Lee, M. Byun, Z.L. Wang, Adv. Mater. 26 (2014) 2514–2520.
[82] T.R. Shrout, S.J. Zhang, J. Electroceram. 19 (2007) 113–126.
[83] Q. He, J. Liu, B. Yang, X. Wang, X. Chen, C. Yang, Sensor Actuator Phys. 219 (2014) 65–72.
[84] Q. Liang, D. Zhang, G. Coppola, Y. Wang, S. Wei, Y. Ge, IEEE Sensor. J. 14 (2014) 2643–2657.
[85] M. Tilli, M. Paulasto-Krockel, T. Motooka, V. Lindroos, Handbook of Silicon Based MEMS Materials and Technologies, William Andrew, 2015.
[86] G. Tang, J.-q. Liu, B. Yang, J.-b. Luo, H.-s. Liu, Y.-g. Li, C.-s. Yang, D.-n. He, V. D. Dao, K. Tanaka, J. Micromech. Microeng. 22 (2012), 065017.
[87] Q. Shi, T. Wang, C. Lee, Sci. Rep. 6 (2016) 24946.
[88] Q. Shi, T. Wang, T. Kobayashi, C. Lee, Appl. Phys. Lett. 108 (2016) 193902.
[89] D.B. Christensen, S. Roundy, J. Intell. Mater. Syst. Struct. 27 (2016) 1092–1105.
[90] H. Peng, X. Sun, W. Weng, X. Fang, Polymer Materials for Energy and Electronic Applications, Academic Press, 2016.
[91] K.S. Ramadan, D. Sameoto, S. Evoy, Smart Mater. Struct. 23 (2014), 033001.
[92] F. Narita, M. Fox, Adv. Eng. Mater. 20 (2018) 1700743.
[93] Z. Pi, J. Zhang, C. Wen, Z.-b. Zhang, D. Wu, Nano Energy 7 (2014) 33–41.
[94] X. Chen, X. Han, Q.D. Shen, Adv. Electron. Mater. 3 (2017) 1600460.
[95] W. Liu, X. Cheng, X. Fu, C. Stefanini, P. Dario, Microelectron. Eng. 88 (2011) 2251–2254.
[96] P.G. De Deyne, M. Kirsch-Volders, Phys. Ther. 75 (1995) 629–634.
[97] S. Roundy, P.K. Wright, J.M. Rabaey, Energy Scavenging for Wireless Sensor Networks, Springer, Norwell, 2003, pp. 45–47.
[98] S. Islam, A. Kim, in: 2018 IEEE International Microwave Biomedical Conference (IMBioC), IEEE, 2018, pp. 70–72.
[99] T. Zheng, J. Wu, D. Xiao, J. Zhu, Prog. Mater. Sci. 98 (2018) 552–624.
[100] S.R. Anton, A. Erturk, D.J. Inman, IEEE Trans. Ultrason. Ferroelectrics Freq. Contr. 59 (2012) 1085–1092.
[101] F. Li, D. Lin, Z. Chen, Z. Cheng, J. Wang, C. Li, Z. Xu, Q. Huang, X. Liao, L.-Q. Chen, Nat. Mater. 17 (2018) 349–354.
[102] L. Jiang, J. Xing, Z. Tan, J. Wu, Q. Chen, D. Xiao, J. Zhu, J. Mater. Sci. 51 (2016) 4963–4972.
[103] L. Jiang, Y. Yang, R. Chen, G. Lu, R. Li, J. Xing, K.K. Shung, M.S. Humayun, J. Zhu, Y. Chen, Q. Zhou, Adv. Funct. Mater. (2019) 1902522.
[104] L. Jiang, Z. Tan, L. Xie, Y. Li, J. Xing, J. Wu, Q. Chen, D. Xiao, J. Zhu, J. Eur. Ceram. Soc. 38 (2018) 2335–2343.

[105] P. Kabakov, C. Dean, V. Kurusingal, Z. Cheng, H.-Y. Lee, S. Zhang, J. Mater. Chem. C 8 (2020) 7606–7649.
[106] D. Seo, J.M. Carmena, J.M. Rabaey, M.M. Maharbiz, E. Alon, J. Neurosci. Methods 244 (2015) 114–122.
[107] J. Charthad, M.J. Weber, T.C. Chang, A. Arbabian, IEEE J. Solid State Circ. 50 (2015) 1741–1753.
[108] K. Ren, Y. Liu, X. Geng, H.F. Hofmann, Q.M. Zhang, IEEE Trans. Ultrason. Ferroelectrics Freq. Contr. 53 (2006) 631–638.
[109] W.A. Smith, B.A. Auld, IEEE Trans. Ultrason. Ferroelectrics Freq. Contr. 38 (1991) 40–47.
[110] Z.-Y. Shen, Y. Xu, J.-F. Li, J. Appl. Phys. 105 (2009) 104103.
[111] V.F. Janas, A. Safari, J. Am. Ceram. Soc. 78 (1995) 2945–2955.
[112] S. Kapuria, P. Kumari, J. Nath, Acta Mech. 214 (2010) 31–48.
[113] Z. Yang, H. Wang, C. Zhao, D. Zeng, Phil. Mag. Lett. 95 (2015) 324–332.
[114] Z. Yang, D. Zeng, H. Wang, C. Zhao, J. Tan, Smart Mater. Struct. 24 (2015), 075029.
[115] Y. Sun, X. Gao, H. Wang, Z. Chen, Z. Yang, Appl. Phys. Lett. 112 (2018), 043903.
[116] L. Jiang, Y. Yang, R. Chen, G. Lu, R. Li, D. Li, M.S. Humayun, K.K. Shung, J. Zhu, Y. Chen, Q. Zhou, Nano Energy 56 (2019) 216–224.
[117] Y. Zhang, C.K. Jeong, J. Wang, H. Sun, F. Li, G. Zhang, L.-Q. Chen, S. Zhang, W. Chen, Q. Wang, Nano Energy 50 (2018) 35–42.
[118] J. Rödel, W. Jo, K.T. Seifert, E.M. Anton, T. Granzow, D. Damjanovic, J. Am. Ceram. Soc. 92 (2009) 1153–1177.
[119] S. Priya, S. Nahm, Lead-free Piezoelectrics, Springer Science & Business Media, 2011.
[120] R. Chen, L. Jiang, T. Zhang, T. Matsuoka, M. Yamazaki, X. Qian, G. Lu, A. Safari, J. Zhu, K.K. Shung, IEEE (Inst. Electr. Electron. Eng.) Trans. Biomed. Eng. 66 (2018) 1580–1587.
[121] M. Pecht, Y. Fukuda, S. Rajagopal, IEEE Trans. Electron. Packag. Manuf. 27 (2004) 221–232.
[122] C.K. Jeong, J.H. Han, H. Palneedi, H. Park, G.-T. Hwang, B. Joung, S.-G. Kim, H. J. Shin, I.-S. Kang, J. Ryu, Apl. Mater. 5 (2017), 074102.
[123] L. Jiang, Y. Li, J. Xing, J. Wu, Q. Chen, H. Liu, D. Xiao, J. Zhu, Ceram. Int. 43 (2017) 2100–2106.
[124] J. Xing, Z. Tan, L. Jiang, Q. Chen, J. Wu, W. Zhang, D. Xiao, J. Zhu, J. Appl. Phys. 119 (2016), 034101.
[125] L. Jiang, Z. Tan, J. Xing, J. Wu, Q. Chen, W. Zhang, D. Xiao, J. Zhu, J. Mater. Sci. Mater. Electron. 27 (2016) 9812–9820.
[126] J. Xing, Z. Tan, X. Chen, L. Jiang, W. Wang, X. Deng, B. Wu, J. Wu, D. Xiao, J. Zhu, Inorg. Chem. 58 (2018) 428–438.
[127] J. Xing, L. Jiang, C. Zhao, Z. Tan, Q. Xu, J. Wu, Q. Chen, D. Xiao, J. Zhu, J. Materiomics 6 (2020) 513–522.
[128] H.L.W. Chan, J. Unsworth, IEEE Trans. Ultrason. Ferroelectrics Freq. Contr. 36 (1989) 434–441.
[129] L. Li, N.R. Sottos, J. Appl. Phys. 77 (1995) 4595–4603.
[130] G. Celler, S. Cristoloveanu, J. Appl. Phys. 93 (2003) 4955–4978.
[131] S. Cristoloveanu, S. Li, Electrical Characterization of Silicon-On-Insulator Materials and Devices, Springer Science & Business Media, 2013.
[132] K. De Vos, I. Bartolozzi, E. Schacht, P. Bienstman, R. Baets, Optic Express 15 (2007) 7610–7615.
[133] J.K. Doylend, M. Heck, J.T. Bovington, J.D. Peters, L. Coldren, J. Bowers, Optic Express 19 (2011) 21595–21604.
[134] Y. Zhu, S.R. Moheimani, M.R. Yuce, IEEE Sensor. J. 11 (2010) 155–161.
[135] A. Fowler, S. Moheimani, S. Behrens, in: Journal of Physics: Conference Series, IOP Publishing, 2013, 012002.
[136] A.G. Fowler, S. Moheimani, S. Behrens, J. Microelectromech. Syst. 23 (2014) 1454–1462.
[137] T. Szabó, O. Berkesi, P. Forgó, K. Josepovits, Y. Sanakis, D. Petridis, I. Dékány, Chem. Mater. 18 (2006) 2740–2749.
[138] A. Lerf, H. He, M. Forster, J. Klinowski, J. Phys. Chem. B 102 (1998) 4477–4482.
[139] Y. Liu, D. Yu, C. Zeng, Z. Miao, L. Dai, Langmuir 26 (2010) 6158–6160.
[140] P. Yao, P. Chen, L. Jiang, H. Zhao, H. Zhu, D. Zhou, W. Hu, B.H. Han, M. Liu, Adv. Mater. 22 (2010) 5008–5012.
[141] C.-T. Hsieh, S.-M. Hsu, J.-Y. Lin, H. Teng, J. Phys. Chem. C 115 (2011) 12367–12374.
[142] S. Park, J. An, I. Jung, R.D. Piner, S.J. An, X. Li, A. Velamakanni, R.S. Ruoff, Nano Lett. 9 (2009) 1593–1597.
[143] R. Que, Q. Shao, Q. Li, M. Shao, S. Cai, S. Wang, S.T. Lee, Angew. Chem. Int. Ed. 51 (2012) 5418–5422.
[144] L. Valentini, S. Bittolo Bon, J.M. Kenny, ACS Appl. Mater. Interfaces 5 (2013) 3770–3775.
[145] Z. Liu, J.T. Robinson, X. Sun, H. Dai, J. Am. Chem. Soc. 130 (2008) 10876–10877.
[146] D. Stauffer, A. Aharony, London 181pp, (1992).
[147] B. Bera, Imper. J. Interdiscipl. Res. 2 (2016) 1263–1271p.
[148] Z.L. Wang, T. Jiang, L. Xu, Nano Energy 39 (2017) 9–23.
[149] F. Yi, Z. Zhang, Z. Kang, Q. Liao, Y. Zhang, Adv. Funct. Mater. 29 (2019) 1808849.
[150] J. Yang, J. Chen, Y. Liu, W. Yang, Y. Su, Z.L. Wang, ACS Nano 8 (2014) 2649–2657.
[151] M. Conte, A. Igartua, Wear 296 (2012) 568–574.
[152] J. Wang, F. Yan, Q. Xue, Wear 267 (2009) 1634–1641.
[153] R. Hinchet, H.-J. Yoon, H. Ryu, M.-K. Kim, E.-K. Choi, D.-S. Kim, S.-W. Kim, Science 365 (2019) 491–494.
[154] A. Yu, X. Chen, R. Wang, J. Liu, J. Luo, L. Chen, Y. Zhang, W. Wu, C. Liu, H. Yuan, ACS Nano 10 (2016) 3944–3950.
[155] N. Cui, L. Gu, J. Liu, S. Bai, J. Qiu, J. Fu, X. Kou, H. Liu, Y. Qin, Z.L. Wang, Nano Energy 15 (2015) 321–328.
[156] X. Wei, J. Liu, Front. Energy Power Eng. China 2 (2008) 1–13.
[157] E. Cingolani, J.I. Goldhaber, E. Marbán, Nat. Rev. Cardiol. 15 (2018) 139.
[158] T. Maleki, N. Cao, S.H. Song, C. Kao, S.-C. Ko, B. Ziaie, IEEE (Inst. Electr. Electron. Eng.) Trans. Biomed. Eng. 58 (2011) 3104–3111.
[159] G.G. Genchi, L. Ceseracciu, A. Marino, M. Labardi, S. Marras, F. Pignatelli, L. Bruschini, V. Mattoli, G. Ciofani, Adv. Healthc. Mater. 5 (2016) 1808–1820.
[160] D.K. Piech, J.E. Kay, B.E. Boser, M.M. Maharbiz, in: 2017 39th Annual International Conference of the IEEE Engineering in Medicine and Biology Society (EMBC), IEEE, 2017, pp. 221–225.
[161] L. Vannozzi, L. Ricotti, C. Filippeschi, S. Sartini, V. Coviello, V. Piazza, P. Pingue, C. La Motta, P. Dario, A. Menciassi, Int. J. Nanomed. 11 (2016) 69.
[162] X. Fan, J. Chen, J. Yang, P. Bai, Z. Li, Z.L. Wang, ACS Nano 9 (2015) 4236–4243.
[163] Y. Wang, X. Wen, Y. Jia, M. Huang, F. Wang, X. Zhang, Y. Bai, G. Yuan, Y. Wang, Nat. Commun. 11 (2020) 1–11.
[164] S. Borchers, M. Himmelbach, N. Logothetis, H.-O. Karnath, Nat. Rev. Neurosci. 13 (2012) 63–70.
[165] J. Jacobs, J. Miller, S.A. Lee, T. Coffey, A.J. Watrous, M.R. Sperling, A. Sharan, G. Worrell, B. Berry, B. Lega, Neuron 92 (2016) 983–990.
[166] S. Danti, G. Ciofani, S. Moscato, D. D'Alessandro, E. Ciabatti, C. Nesti, R. Brescia, G. Bertoni, A. Pietrabissa, M. Lisanti, Nanotechnology 24 (2013) 465102.
[167] F. Mazzilli, M. Peisino, R. Mitouassiwou, B. Cotté, P. Thoppay, C. Lafon, P. Favre, E. Meurville, C. Dehollain, in: 2010 Annual International Conference of the IEEE Engineering in Medicine and Biology, IEEE, 2010, pp. 3751–3754.
[168] M.A. Nicolelis, D. Dimitrov, J.M. Carmena, R. Crist, G. Lehew, J.D. Kralik, S. P. Wise, Proc. Natl. Acad. Sci. Unit. States Am. 100 (2003) 11041–11046.
[169] D. McDonnall, G.A. Clark, R.A. Normann, IEEE Trans. Neural Syst. Rehabil. Eng. 12 (2004) 208–215.
[170] D.K. Piech, B.C. Johnson, K. Shen, M.M. Ghanbari, K.Y. Li, R.M. Neely, J.E. Kay, J. M. Carmena, M.M. Maharbiz, R. Muller, Nat. Biomed. Eng. 4 (2020) 207–222.
[171] M.R. Prausnitz, R. Langer, Nat. Biotechnol. 26 (2008) 1261.
[172] G. Tiwari, R. Tiwari, B. Sriwastawa, L. Bhati, S. Pandey, P. Pandey, S. K. Bannerjee, Int. J. Pharm. Invest. 2 (2012) 2.
[173] D. Chen, S.K. Sharma, A. Mudhoo, Handbook on Applications of Ultrasound: Sonochemistry for Sustainability, CRC press, 2011.
[174] F. Akhtar, M.H. Rehmani, Renew. Sustain. Energy Rev. 45 (2015) 769–784.
[175] M.G. Roes, J.L. Duarte, M.A. Hendrix, E.A. Lomonova, IEEE Trans. Ind. Electron. 60 (2012) 242–248.
[176] F. Chen, Y. Wu, Z. Ding, X. Xia, S. Li, H. Zheng, C. Diao, G. Yue, Y. Zi, Nano Energy 56 (2019) 241–251.
[177] Q. Zhou, K.H. Lam, H. Zheng, W. Qiu, K.K. Shung, Prog. Mater. Sci. 66 (2014) 87–111.
[178] H. Li, Y. Sang, S. Chang, X. Huang, Y. Zhang, R. Yang, H. Jiang, H. Liu, Z.L. Wang, Nano Lett. 15 (2015) 2372–2379.
[179] P. Zhu, Y. Chen, J. Shi, Adv. Mater. (2020) 2001976.
[180] Y. Zhang, C.-H. Chen, T. He, G.C. Temes, IEEE J. Solid State Circ. 52 (2017) 1066–1076.
[181] Y.-S. Shu, L.-T. Kuo, T.-Y. Lo, IEEE J. Solid State Circ. 51 (2016) 2928–2940.
[182] X. Huang, L. Wang, H. Wang, B. Zhang, X. Wang, R.Y. Stening, X. Sheng, L. Yin, Small (2019) 1902827.
[183] M. Cai, Z. Wang, Y. Luo, S. Mirabbasi, IEEE Trans. Microw. Theor. Tech. 66 (2018) 5129–5140.
[184] M. Zgaren, A. Moradi, L.F. Tanguay, M. Sawan, Int. J. Circ. Theor. Appl. 46 (2018) 2266–2282.
[185] L.S. Wong, S. Hossain, A. Ta, J. Edvinsson, D.H. Rivas, H. Naas, IEEE J. Solid State Circ. 39 (2004) 2446–2456.
[186] I. Dincer, Comprehensive Energy Systems, Elsevier, 2018.
[187] J.T. Heaton, J.B. Kobler, D.M. Otten, R.E. Hillman, S.M. Zeitels, Ann. Otol. Rhinol. Laryngol. 128 (2019) 53S–70S.
[188] Y. Nishio, A. Kobayashi, K. Niitsu, IEICE Trans. Electron. 102 (2019) 269–275.
[189] Y. Lee, B. Giridhar, Z. Foo, D. Sylvester, D. Blaauw, in: 2011 IEEE International Solid-State Circuits Conference, IEEE, 2011, pp. 46–48.
[190] H. Basaeri, Y. Yu, D. Young, S. Roundy, IEEE Sensors Lett. 3 (2019) 1–4.
[191] A. Sawaby, M.L. Wang, E. So, J.-C. Chien, H. Nan, B.T. Khuri-Yakub, A. Arbabian, in: 2018 IEEE Symposium on VLSI Circuits, IEEE, 2018, pp. 189–190.
[192] V. Sivaji, D.W. Grasse, S.A. Hays, J.E. Bucksot, R. Saini, M.P. Kilgard, R. L. Rennaker, II, J. Neurosci. Methods 320 (2019) 26–36.
[193] H. Kang, W.H. Abbasi, S.-W. Kim, J. Kim, Sensors 19 (2019) 536.
[194] S. Anand, J. Sutanto, M.S. Baker, M. Okandan, J. Muthuswamy, J. Microelectromech. Syst. 21 (2012) 1172–1186.
[195] D.A. Christensen, Ultrasonic Bioinstrumentation, wiley, New York, 1988.
[196] D. Pham, M. Al-Kutubi, Z. Ji, M. Yang, Z. Wang, S. Catheline, in: Proceedings of IPROMS 2005 Virtual Conference, Citeseer, 2005, pp. 497–502.
[197] R. Kar-Gupta, T. Venkatesh, Acta Mater. 55 (2007) 1093–1108.
[198] H. Hu, X. Zhu, C. Wang, L. Zhang, X. Li, S. Lee, Z. Huang, R. Chen, Z. Chen, C. Wang, Sci. Adv. 4 (2018), eaar3979.
[199] Z. Chen, Z. Li, J. Li, C. Liu, C. Lao, Y. Fu, C. Liu, Y. Li, P. Wang, Y. He, J. Eur. Ceram. Soc. 39 (2019) 661–687.
[200] Z. Chen, X. Song, L. Lei, X. Chen, C. Fei, C.T. Chiu, X. Qian, T. Ma, Y. Yang, K. Shung, Nano Energy 27 (2016) 78–86.
[201] X. Song, L. He, W. Yang, Z. Wang, Z. Chen, J. Guo, H. Wang, L. Chen, J. Manuf. Sci. Eng. (2019) 141.
[202] Z. Chen, X. Qian, X. Song, Q. Jiang, R. Huang, Y. Yang, R. Li, K. Shung, Y. Chen, Q. Zhou, Micromachines 10 (2019) 170.

[203] J. Black, Biological Performance of Materials: Fundamentals of Biocompatibility, Crc Press, 2005.
[204] P. Panda, B. Sahoo, Ferroelectrics 474 (2015) 128–143.
[205] D.-H. Kim, R. Ghaffari, N. Lu, J.A. Rogers, Annu. Rev. Biomed. Eng. 14 (2012) 113–128.
[206] C. Wang, X. Li, H. Hu, L. Zhang, Z. Huang, M. Lin, Z. Zhang, Z. Yin, B. Huang, H. Gong, Nat. Biomed. Eng. 2 (2018) 687.
[207] Y. Yang, H. Hu, Z. Chen, Z. Wang, L. Jiang, G. Lu, X. Li, R. Chen, J. Jin, H. Kang, Nano Lett. 20 (2020) 4445–4453.
[208] U. Food, D. Administration, Rockville, MD: Center for Devices and Radiological Health, US Food and Drug Administration, 1997.
[209] A.G. Fowler, S.R. Moheimani, S. Behrens, SENSORS, IEEE, 2012, pp. 1–4. IEEE2012.
[210] X. Zhang, J. Liu, M. Chu, B. Chu, Appl. Phys. Lett. 109 (2016), 072903.
[211] Y. Zhang, C.K. Jeong, T. Yang, H. Sun, L.-Q. Chen, S. Zhang, W. Chen, Q. Wang, J. Mater. Chem. 6 (2018) 14546–14552.
[212] Y. Yang, X. Li, X. Zheng, Z. Chen, Q. Zhou, Y. Chen, Adv. Mater. 30 (2018) 1704912.
[213] X. Yuan, X. Gao, J. Yang, X. Shen, Z. Li, S. You, Z. Wang, S. Dong, Energy Environ. Sci. 13 (2020) 152–161.
[214] Y. Yang, Z. Chen, X. Song, B. Zhu, T. Hsiai, P.-I. Wu, R. Xiong, J. Shi, Y. Chen, Q. Zhou, Nano Energy 22 (2016) 414–421.
[215] Y. Yang, X. Li, M. Chu, H. Sun, J. Jin, K. Yu, Q. Wang, Q. Zhou, Y. Chen, Sci. Adv. 5 (2019), eaau9490.
[216] C. Liu, N. Huang, F. Xu, J. Tong, Z. Chen, X. Gui, Y. Fu, C. Lao, Polymers 10 (2018) 629.
[217] Y. Yang, X. Song, X. Li, Z. Chen, C. Zhou, Q. Zhou, Y. Chen, Adv. Mater. 30 (2018) 1706539.

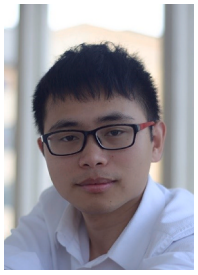

Dr. Laiming Jiang is a Postdoctoral Researcher - Research Associate in the Keck School of Medicine at the University of Southern California (USC). He received his Ph.D. degree in Materials Physics and Chemistry from the Department of Materials Science and Engineering, Sichuan University, in 2019. His research work focuses on lead-free piezoelectric materials, ultrasound transducers/array, energy harvesting, multiscale and multi-materials 3d printing, and bio-implantable devices.

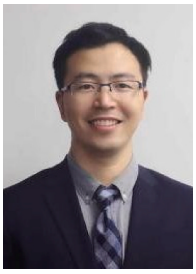

Dr. Yang Yang is an Assistant Professor in the Department of Mechanical Engineering at San Diego State University (SDSU). Prior to joining SDSU, he worked as a postdoctoral research associate at University of Southern California (USC) in the Department of Industrial and Systems Engineering and Center for Advanced Manufacturing. His research is focused on bio-inspired additive manufacturing (3D printing), energy harvesting devices, mechanism of materials and structures, high dielectric nanocomposites and wearable sensors.

Dr. Yong Chen is a Professor in the Epstein Department of Industrial and Systems Engineering and Department of Aerospace and Mechanical Engineering at the University of Southern California (USC). He received his Ph.D. degree in mechanical engineering from Georgia Institute of Technology in 2001. Prior to joining USC in 2006, he was a Senior Research and Development Engineer at 3D Systems Inc. His research focuses on additive manufacturing (3D printing) in micro- and mesoscales, especially the modeling, analysis, synthesis, and optimization of digital design and manufacturing.

Dr. Qifa Zhou received his Ph.D. degree from the Department of Electronic Materials and Engineering at Xi'an Jiaotong University. He is currently a professor of Biomedical Engineering and Ophthalmology at the University of Southern California (USC). Dr. Zhou is a fellow of the Institute of Electrical and Electronics Engineers (IEEE), the International Society for Optics and Photonics (SPIE), and the American Institute for Medical and Biological Engineering (AIMBE). He has published more than 260 peer-reviewed articles in journals. His research focuses on the development of high-frequency ultrasonic transducers/array and photoacoustic imaging as well as multimodality imaging.